2023-04-01

Analyzing drainage basin orientation and its relationship to active fold growth (Handun anticline, Zagros, Iran)

Shahram Bahrami

Martin Stokes *School of Geography, Earth and Environmental Sciences*

Analyzing drainage basin orientation and its relationship to active fold growth (Handun anticline, Zagros, Iran)

Shahram Bahrami[1], Martin Stokes[2]

1- Department of Physical Geography, School of Earth Sciences, Shahid Beheshti University, Tehran, Iran

2- School of Geography, Earth and Environmental Sciences, University of Plymouth, Plymouth, UK

Abstract

Combinations of tectonic geomorphological criteria are frequently used to detect vertical and lateral growth of fold structures in tectonically active settings due to their low cost and relative ease of application. The purpose of this study is to analyze the morphometric properties of drainage basins developed into the flanks of a growing anticline to explore the active tectonic growth patterns of the fold. We target the Handun anticline in the Zagros Simply Folded Belt due to it being actively growing fold structure and that possesses a high variability of drainage basin morphologies across different parts of the fold structure.

57 drainage basins were characterized in terms of their orientation using a newly defined drainage basin orientation (DBO) index, in combination with a set of standard tectonic geomorphological metrics (drainage basin area [Ba], slope [S], asymmetry factor [AF], hypsometric integral [HI], basin shape [Bs], crescentness index [CI], sinuosity of main drainage [Smd], drainage density [Dd], drainage density of 1st-order streams [Dd1], drainage frequency [Df]) and sinuosity of the main anticline ridge [Sad]). Indices were synthesized for spatial comparison between western, central and eastern zones of the growing fold.

Results show that the DBO is strongly correlated with its CI, Smd, and A. In terms of spatial distribution, the central zone (the main fold axis) is characterized by lower values of DBO, A, S, CI, Smd, and Sad. These contrast with the western and eastern zones (fold plunge regions), which are characterized by higher values of Dd, Dd1, and Df. Of note is the southern limb of the anticline, which is characterized by drainage basins with larger A, and higher values of AF, CI, and Smd. This suggests higher lateral erosion on the southern fold flanks. In contrast, drainage basins with steeper S, and greater DBO elongation are found on the northern limb, suggesting dominance of vertical erosion. This contrasting south-north erosion pattern suggests that the northern fold flank is actively steepening, and presenting a more youthful topography, with lower and spatially focused erosion that is increasing with time. Overall, high values of the newly proposed DBO metric relate to the presence of a curved and / or an asymmetric forked drainage pattern that is configured to the trend of faults and fractures across the fold. These structures are typically oriented oblique to the fold axis, with further modification into a semi-annular drainage pattern developed around a salt diapir.

Keywords: Drainage basin orientation, tectonic geomorphological indices, folds, anticlines

Introduction

Quantitative analysis of landforms in tectonically active regions, especially within collisional zones of elevated compressive strain, can provide useful information concerning the patterns and rates of tectonic activities and the landscape development (Jackson et al., 1998; Delcaillau et al., 2006; Ramsey et al., 2008; Keller and DeVecchio, 2022). Such analysis can be achieved through application of geomorphic indices to the landscape and its component landforms. These DEM and satellite images derived indices are low-cost, with relatively easy-to-perform data collection and analysis steps. Thus, they are highly effective tools to apply and inform on improving our understanding of active tectonics. Morphometric parameters related to drainage basins (i.e., hypsometric integral, asymmetry, elongation, circularity, crescentness index), river networks (i.e., drainage density, frequency, confluence angle, hierarchal anomaly index), and mountain fronts (i.e., mountain front sinuosity, facet slope-to-height ratio, percentage faceting, valley floor width-to-height ratio) have been commonly applied to landscapes affected by varying tectonic activity worldwide (Wells et al., 1988; Ramírez-Herrera, 1998; El Hamdouni et al., 2008; Peréz-Peña et al., 2010; Altin and Altin, 2011; Özkaymak and Sözbilir, 2012; Bahrami, 2013; Bahrami et al., 2020; García-Delgado and Velandia, 2020; Różycka and Migoń, 2021; Bahrami, 2022). In compressional tectonic settings, the geomorphic signatures of a laterally growing (widening) fold typically includes: (1) decreases in drainage density and degree of dissection; (2) decrease in elevation of wind gaps; (3) decrease in relief along a fold topographic profile; (4) development of asymmetric drainage patterns; (5) deformation of progressively younger deposits or landforms; (6) decrease in rotation and inclination of the anticline forelimb; (7) development of an asymmetric forked tributary network; (8) development of a series of curved wind gaps; and (9) the development of fan-shaped tributary drainage patterns on fold flanks, have all been analyzed in folded structures (Keller et al., 1999; Ramsey et al., 2008; Bretis et al., 2011; Keller and DeVecchio, 2013; Collignon et al., 2015, 2016;Sissakian et al., 2019; Machuca et al., 2021; Adeoti and Webb, 2022). Nevertheless, little attention has been devoted to the drainage basin orientation and its relation to active tectonics in growing folds. The few existing studies include Ramsey et al. (2007) who evaluated the deflection of rivers using the angle between the general trend of the basin outlet with respect to an east-west direction. They suggested that deflections of rivers are controlled by the fault lines. A further example is by Krystopowicz et al. (2020) who defined a morphometric factor, called the catchment-fault azimuth, expressed as the angle between the fault and the main axis of the catchment measured in a counterclockwise direction. Their study revealed that values of basin asymmetry and basin-fault azimuth illustrate tilting of fault block footwall catchments as part of a regional tilting pattern. Generally, the trunk drainage of a basin is oriented perpendicular to the mountain front line, whereas it is oriented oblique to the mountain front line, or fold axis, when it is affected by a fault trace or lateral growth of a fold. Thus, quantitative evaluation of the orientation of drainage basins developed on the fold flanks can obtain useful information about active tectonics.

The Zagros Simply Folded belt is one of the most tectonically active areas in the world, containing pronounced 'whaleback' anticlines that are growing vertically and laterally (Lee and Falcon, 1952; Berberian, 1995; Ramsey et al., 2008; Bahrami, 2013; Faghih and Nourbakhsh, 2014; Collignon et al., 2016; Woodbridge et al., 2019; Bahrami, 2022). Although drainage system development and morphometry have been studied as evidence of fold growth throughout the Zagros (Ramsey et al., 2008; Bretis et al., 2011; Bahrami, 2013; Collignon et al., 2016; Woodbridge et al., 2019; Bahrami et al., 2020), drainage basin orientation in association with vertical and lateral growth of folds is a less evaluated aspect. Recently, Bahrami et al. (2020) proposed a "crescentness index" of a drainage basin as a new morphometric index suggesting lateral growth of the Gorm anticline (Fars region). The study showed that the development of crescent-shaped basins in the pre-nose fold segment, where the upstream drainage basin parts have been curved towards the central region of the anticline, provides strong geomorphic evidence for lateral fold propagation. In terms of the Handun anticline which forms the focus of this study, Ramsey et al. (2008) briefly examined the effect of some oblique fractures on the orientation and pattern of its drainages. However, detailed examination and precise interpretation of its drainage basin morphometries and their networks across different parts of the Handun anticline have not been considered. The Handun anticline displays a high variability in the morphometry of its drainage basins and their networks, and we use this variability to explore in detail and more precisely their relationships to tectonic activity.

Accordingly, the objectives of this study are to: (1) investigate the relationship between drainage basin orientation and the morphometric properties of the drainage basins and their networks; (2) to assess the variations of the analyzed morphometric parameters in three tectonic zones and the northern and southern limb flanks of the growing fold structure; and (3) evaluate the effects of lateral and vertical growth of the fold and its resulting fault trends on the drainage basin orientation.

Study area

Geological setting

The Zagros Fold and Thrust Belt (ZFTB), in which the study area is located, is one of the youngest continental collision belts in the world, extending over 1500 km from Kurdistan in northern Iraq to the Hormuz Strait at the mouth of the Persian Gulf. Folding in the Zagros Simply Folded Belt started in the early Miocene (Sherkati et al., 2005), and folds associated with the Zagros Foredeep are still growing (Berberian, 1995).

The Handun anticline is part of Bandar Abass region in the eastern termination of the ZFTB.

The Bandar Abbas region, also known as the hinterland, syntaxis, and embayment is a transitional area between three geological zones comprising 1) the Zagros collisional belt to the NW, 2) the Makran accretionary prism to the east, and 3) the Oman Mountains to the SE (Molinaro et al., 2004; Faridi et al., 2021). Two main characteristics of the eastern Zagros are: (1) numerous emergent or still buried salt diapirs, distributed irregularly across a wide region from the suture zone in the north to the Persian Gulf in the south; and (2) particular aspect ratios of folds, which are typically short and (compact) folds with irregular along strike shapes that frequently display a plan view ‘zigzag’ shape on maps and satellite imagery with marked changes in fold axis configuration (Jahani et al., 2009).

The Handun anticline in the Zagros Simply Folded Belt (ZSFB), located to the northeast of the town of Fin in the Hormozgan province (Fig. 1) is the focus of this study. The anticline is oriented E-W, with a length of 37 km, width of 9 km and area of 244.5 km^2. The anticline spans an altitudinal range from 1840 m to 280 m. The Middle Miocene to Pleistocene syn-orogenic coarsening upward sediments of the Agha Jari and Bakhtiyari Formations developed in central parts of the Handun anticline show the minimum age of anticline is Pleistocene (Faridi et al., 2021).

Lithological units of the anticline span the Pre-Cambrian, Cenozoic and the Quaternary (Fig. 2). The areas of Guri, Razak, Asmari-Jahrom, Hormuz, Quaternary, and Bakhtyari formations are respectively 80%, 7.2%, 6.4%, 4.7%, 1.6%, and 0.1% of the whole study area. Two sets of faults crosscut the Handun anticline, including (1) E-W trending faults, parallel to the fold axis; and (2) NW-SE trending faults, oblique to the fold axis (Fig. 2). The Handun anticline occurs within a zone of relatively high seismic activity (Berberian and Tchalenko, 1976). Some historical and twentieth-century earthquakes have been recorded in the Bandar Abbas region (Berberian et al., 1977; Berberian and Tchalenko, 1976; Ambraseys and Melville, 1982; Berberian, 2014; Zare et al., 2014). Notable events include the Khurgu earthquake (21 March 1977 Mw 7), as one of the most destructive earthquakes in the Bandar Abbas region, occurring ~ 15 km southeast of the Handun anticline.

Folds in the western branch of the syntaxis, in which the Handun anticline is located, have higher aspect ratios (half wavelength/axial length), compared to the eastern branch of the syntax which comprises long and thin folds with lower aspect ratios (Molinaro et al., 2004). The Handun anticline is a faulted detachment fold (Molinaro et al., 2005, Ginés et al., 2019; Faridi et al., 2021) with a salt core. In the Southeastern Zagros Folded belt, the Hormuz Series, composed predominantly of the Late Precambrian Hormuz Salt formation (1–1.5 km-thick), forms a basal viscous decollement influencing the wavelength, amplitude and style of folding

(Colman-Sadd, 1978; Sepehr and Cosgrove, 2004). According to Molinaro et al. (2004, 2005), folding developed first through the development of large detachment anticlines, followed by steep limbs of the most developed folds in the Southeastern Zagros that have already reached a more mature stage involving faulting within the forelimbs of the folds.

The Handun anticline comprises a salt diapir located at the fold culmination, exhibits a particular ‘peanut-like’ shape in plan view (Jahani et al., 2009). According to Jahani et al. (2009) the Handun diapir is now inactive with a wide empty crater, but shows growth strata in the Eocene-Oligocene levels and recycled Hormuz materials in Miocene beds, implying that the plug was near the surface before the Zagros orogeny and then emerged during folding. Due to the relative weakness of the salt and the strength of the surrounding wall-forming rocks, a strain gradient develops so that the central portion of the wall is squeezed more than the ends. With further fold shortening, a vertical weld develops, linking two remnant diapirs that have not been squeezed as much (Rowan and Vendeville, 2006). The core of Handun anticline is broken through by a salt diapir whose emergent top surface is now eroded away. According to the classification of salt diapirs of Eastern Fars based on their present-day surface morphology (Jahani et al., 2007), the Handun salt diapir is ‘dead’, comprising a highly eroded dome located within a near empty crater (type E: *sensu* Janhani et al., 2007).

Based on the Bandar Abbas synoptic station located approximately 50 km southeast of the study area, the mean annual precipitation, temperature and relative humidity (during 1980-2021 period) are 169.2 mm, 26.9 °C and 64.6%, respectively.

Geomorphic features

Based on the dip, topographic slopes, and width of limbs, the Handun anticline can be divided into 3 tectonic zones: western (W), central and eastern (E). The W and E zones encompass the plunges of the anticline, whereas the central zone comprises the main anticlinal ridge and its limbs which are extensively eroded. In the western and eastern zones, the flanks of the plunging anticlinal limbs are incised by numerous low order consequent drainages and, in some cases, their orientation is changed by the fracture trends. As described by Ramsey et al. (2008), two wind gaps (abandoned / isolated dry valleys) are developed in the western plunge of the fold. The larger wind gap occurs as a ~ 5-km-long and 200-m-deep dry valley across the fold crest with several meanders. The second wind gap in the west comprises a shorter and straighter valley, cutting the tip of the fold. A 3rd wind gap can also be identified around the western nose of the anticline, where a deflected river around the fold nose has left a shallow wind gap (Fig. 3). Topographic cross-sections along the crest (AA′ profile), across the width of the fold (BB′, CC′, DD′, and EE′ profiles), and parallel to the hinge in the northern and southern limbs (FF′ and GG′) are shown in Fig. 4. The crest profile shows significant erosion of the central fold region, resulting in the formation of larger and more circular basins, especially on the southern limb. Transverse profiles across the fold demonstrate that the southern limb is more eroded compared to the northern one (BB′, and DD′ profiles). The plunged zones (BB′ and EE′ profiles) have gentler topographic gradients. However, these two display differences, where the eastern plunge (EE′) is more eroded compared to the western one (BB′). Profiles parallel to thehinge in the northern and southern limbs (FF′ and GG′) show higher erosion and entrenchment of the southern limb compared to the northern one. Evaluation of the fold crest line (Fig. 6) shows that the central part of the anticline is extensively eroded compared to the plunged zones, indicated by higher sinuosity along the anticline divide in the center, and lower values in the western and eastern zones (Table 1).

The combined effect of uplift and erosion of anticline has resulted in the formation of triangular facets along the southern limb of the central zone (Fig. 5). Erosion of these triangular facets acting concurrently with uplift of the mountain fronts has created V-shaped valleys, with their wide upper parts and narrow outlets, known as 'wine-glass' forms on the steep slopes of southern limb in the central portion of the anticline (Fig. 5a). Surface features of karst, especially karren, are common geomorphic features on carbonate rocks of the Guri Member (Fig. 5b).

Materials and methods

Faults, stratigraphic units, their lithologies and their collective spatial distributions were derived from 1:100,000-scale geological maps (Gharabeili, 2005; Talebi, 2007). 57 drainage basins developed into the anticline limbs were delineated based on Google Earth™ images and 12.5 m resolution ALOS DEM data. Note that the 57 drainage basins are the main rivers whose trunk streams originate at the main drainage divide of the anticline. Drainage networks were digitized manually using Google Earth™ images in combination with the 12.5 m ALOS DEM. The mapped drainages were ordered according to Strahler system (Strahler, 1957) (Fig. 6).

Generally, the water flow direction is perpendicular to the contour lines, and hence the main drainage networks flow perpendicular to the fold axis ((Jackson et al., 1998; Ramsey et al., 2008). The main drainage network of a basin, formed on a fold flank, is oriented at a high angle to the mountain front (close to 90º), whereas it is oriented oblique to the mountain front line, or fold axis, when it is affected by a fault trace or lateral growth of a fold (Ramsey et al., 2007; Ramsey et al., 2008; Ribolini and Spagnolo, 2008; Castelltort et al., 2012; Krystopowicz et al., 2020)

Thus, the degree of oblique orientation of the drainages with respect to the mountain front can be diagnostic of active tectonic controls. In this study, a new geomorphic index, namely the drainage basin orientation (DBO), is presented to evaluate the effect of active tectonics in controlling the orientation of drainage developed into the flanks of an anticline. The DBO is defined as:

$$DBO = |90 - \alpha|$$

where α is the angle between the mountain front line and the straight-line between the endpoints of basin's main drainage (Fig. 7a). High values of DBO (i.e., larger than 15^{o}) reflect basins affected by active tectonics such as faulting and lateral growth of folds. Very low DBO values (close to 0) typically demonstrate 'normal' drainage basins little affected by active tectonics. However, in some rare cases, drainage basins with lower DBO values (close to 0) can be affected by faults trending perpendicular to the fold axis.

As a fold grows, all of the morphometric properties of drainage basins and their networks are affected by active tectonics. In addition to the DBO index, other morphometric indices related to drainage basins and their networks are used in this study: area (Ba), slope (S), asymmetry factor (AF), hypsometric integral (HI), basin shape (Bs), crescentness index (CI), sinuosity of main drainage (Smd), drainage density (Dd), drainage density of 1st-order streams (Dd1), drainage frequency (Df), and sinuosity of anticline divides (Sad). The area and slope of drainage basins were calculated using Integrated Land and Water Information System (ILWIS 3.3) software (ITC, 2007). The mean topographic slope (%) of each basin (S) was derived by weighted average of all pixels of the slope map. The basin mid-lines were obtained using the 'Distance Calculation' function in the ILWIS software. The asymmetry factor (AF) is used to calculate possible tectonic tilting of a drainage basin (Hare and Gardner, 1985; Keller and Pinter, 2002; El Hamdouni et al., 2008). It is defined as: AF = 100(Ar/At), where Ar is the drainage area on the right hand (facing downstream) of the main stream and At is the total area of the drainage basin. In this study, the AF is expressed as the absolute value minus 50 (Peréz-Peña et al., 2010):

$$AF = \left| 50 - \frac{Ar \times 100}{At} \right|$$

The basin shape (Bs) index is expressed as: Bl/Bw

where Bl is the length of basin mid-line and Bw is the width of the basin measured at its widest point (see details in Bahrami et al., 2020). Drainage basins in tectonically active areas are generally considered youthful and actively eroding and thus possess an elongated shape (higher Bs value) (Ramírez-Herrera, 1998).

Drainage density (Dd) is defined as total stream length per unit area (Horton, 1932; Langbein, 1947). Drainage frequency is the total number of stream segments of all orders per unit area (Devi et al., 2011). The first-order drainages are sensitive to tectonics and are important indicators of areas with high rates of uplift (Zuchiewicz, 1998; Keller and Pinter, 2002). The N1/N index, the ratio of 1st-order streams to the total number of streams of all orders, is expected to increase in younger segments (plunges) of a laterally growing anticline. Drainage density, drainage frequency, and the N1/N indexes can provide insights into the impact of active tectonics on drainage networks (Devi et al., 2011; Melosh and Keller, 2013, Bahrami, 2022). In the older segments of tectonically active folds, drainage density and frequency are more developed and have had more time to integrate or cannibalize other nearby drainages, whereas the number of low-order streams are higher in the younger segments (noses) (Keller and Pinter, 2002, Bahrami et al., 2020).

Sinuosity of main drainage (Smd) of a basin is expressed as:

Smd= Mc/SL

where Mc is the length of the main channel and SL is the length of the straight-line between the endpoints of the main channel (Fig. 7b). The rate of uplift and slope gradient can affect the values of channel sinuosity (Adams, 1980; Zámolyi et al., 2010; Joshi et al., 2013). It is expected that channel sinuosity is higher in the older and more uplifted segment of the anticline due to the higher lateral erosion of basins, whereas it is lower in the younger segments (noses) due to the presence of younger basins with lower erosion.

The hypsometric integral (HI) is calculated using an elevation-relief ratio (Strahler, 1952; Delcaillau et al., 1998; Bishop et al., 2002; Pavano et al., 2018). In this study, the 2nd order polynomial equation was fitted to the hypsometric curve, and then the fitted equation was integrated within the desired limits (0 to 1) to estimate the HI (Harlin, 1978; Singh et al., 2008; Liffner et al., 2018; Bahrami et al., 2020). High HI values typically reflect pronounced 'youthful' topography, likely corresponding to recent tectonic deformation. Low HI values are often related to 'older' landscape topography that has been exposed and thus eroded for a longer time period (Keller and Pinter, 2002; He et al., 2019).

The crescentness index (CI) (Bahrami et al., 2020) is defined as:

$$CI=LBM/SL$$

where LBM is the length of the basin mid-line and SL is the length of the straight-line between the endpoints of basin mid-line (Fig. 7c. High CI values (close to 1.5) are associated with entirely crescent-shaped basins, whereas the low CI values (close to 1) are straight basins (least crescent-shaped). The higher CI values relate to drainage basins developed on fold limbs, and these are considered as evidence for lateral fold growth (Bahrami et al., 2020).

Sinuosity of anticline divides (Sad) is a quantitative index related to fold morphometry. In the early stages of fold formation, the main drainage divide usually coincides with the fold hinge. As the fold grows over time, headward erosion of the basins formed on the fold limb flanks will increase the sinuosity of the fold main drainage divide, hence forcing divergence between the hinge and the main topographic divide. The 'Sad' is defined as (Bahrami et al., 2020):

Sad = LD/LH

where LD is the length of main divide of the anticline and LH is the hinge length (Fig. 7d). Generally, higher Sad values are associated with the older, more eroded segment of the anticline (core), whereas lower values are related to younger segments (noses) with lower erosion.

To analyze correlations between variables, the Pearson's correlation coefficient (r) and probability at 0.01 and 0.05 levels for the utilized morphometric parameters were calculated. In order to compare the means of variables in two groups of basins (Northern limb/Southern limb basins), the independent sample t-tests were calculated for different parameters. Tukey's post -hoc test was performed to show statistically significant differences between pairs of means (Zone1 versus zone 2, zone 1 versus zone 3, and zone 2 versus zone 3) for different parameters.

The rock strength also plays a role in the morphometry of landforms and drainage networks (Stokes and Mather, 2015). Although most of the study area (80%) is composed of the same lithology (Guri Member), the exposure of some lithological units having various strengths in the study area could exert some effect upon the morphometry of the basins and their drainage networks. According to some studies focused on the relative strength of geological formations in Iran (Sepehr and Honarmandnejad, 2012; Peyrowan and Shariatjafari, 2013), we categorized the lithological formations of the study area into two strength types:

Type 1 (strong): Guri, Asmari–Jahrom, Bakhtiari,

Type 2 (weak): Hormuz Series, Razak, and Quaternary alluvial terraces and deposits

Basins that comprised >70% of type 1 were considered to have a 'strong' rock strength, 50 to 70% type 1 as 'intermediate' strength, and <50% type 1 as 'weak' strength.

Results

Rates and variations of parameters

The study area anticline and its 57 drainage basins across the three tectonic zones are shown in Fig. 8. The morphometric properties of the studied drainage basins are summarized in Table 5. Values of basin area range from 0.058 km^2 (basin 40 in the eastern zone) to 25.74 km^2 (basin 45 in the central zone). Amongst all basins, basin 1 (western zone) has the lowest topographic slope (8.5%), whereas basin 34 (central zone) has the highest value (69.27%). Basin 7 (western zone) is the most elongated (Bs= 11.43), whereas basin 31 (central zone) is the most circular (Bs=1.165). The lowest HI value (0.41) is associated with basin 40 (eastern zone) whereas the highest HI value (0.77) is related to basin 17 (western zone). The lowest value of asymmetry factor (0.81 %) is related to basin 31 (central zone), and the highest value (35.2%) is associated with basin 22 (western zone). Basin 1 (western zone) has lowest value of the crescentness index (CI= 1.003) whereas basin 35 (central zone) is the most crescent-shaped (CI=1.344). The lowest value of sinuosity of the main drainage (1.028) is associated with basin 56 (in the western zone) whereas the highest value (2.57) is related to basin 52 (western zone). Values of drainage basin orientation across the study area ranges from 0 (basin 30 in the central zone) to 46° (basin 45 in the central zone).

Tectonic zone results

The values of the morphometric parameters of the drainage networks (Dd, Dd1, and Df), the mean values of drainage basin properties (Ba, S, Bs, HI, AF, CI, Smd, and DBO), and the sinuosity of the anticline drainage divide (Sad) across the 3 tectonic zones are given in Table 1. Results show that basins have a larger mean area in the central zone (4.02 km^2), compared to the western and eastern zones (respectively 1.93 and 1.73 km^2). The mean of topographic slope of basins in the central zone (54.81%) is higher compared to the western and eastern zones (23.25% and 31.3% respectively). The central zone has relatively circular basins compared to more elongated basins in the western and eastern zones. This is confirmed by the lower mean value of Bs in the central zone (2.46) compared to higher mean Bs in the western and eastern zones (5.34 and 4.58 respectively). Higher mean HI values in the western zone (0.63), compared to those of the central and eastern zones (0.53 and 0.46 respectively) shows that basins of the western zone have younger topography than other zones. Basins have higher mean values of AF in the western zone (15.31), compared to the central and eastern zones (12.48 and 5.53 respectively). Although the absolute value of AF increases from the western zone towards the eastern zone, a regular trend in the direction of basin tilting is lacking. About 60% of basins in the western zone are tilted towards the west, whilst 50% of basins in the central zone are tilted towards the west, and 67% of basins in the eastern zone are tilted towards the north. The mean crescentness index (CI) is higher the central zone (1.13), compared to the western and eastern zones (1.09 and 1.04 respectively). The mean sinuosity of main drainage (Smd) of basins is higher in the central zone (1.24) than the western and eastern zones (1.19 and 1.16 respectively). The mean drainage basin orientation (DBO) is also higher in the central zone (24.36o), compared to the western and eastern zones (22 o and 13.67 o respectively). Results of the sinuosity of the anticline divide (Sad) show that the central zone of the anticline is characterized by higher Sad values (1.37) compared to the northwestern and southeastern noses (1.23 and 1.03 respectively).

As Fig. 9 shows, the median values of Ba, S, CI, and DBO are greater in the central zone compared to western and eastern zones. In contrast, the median value of Bs is lower in the central zone compared to the plunges. The median values of AF and HI decrease from western zone towards eastern zone. The median values of Smd are fairly similar among three zones.

The ANOVA test results (Table 2) show that means of basin slope, basin shape, hypsometric integral, and asymmetry factor have statistically significant differences between three zones. Results of Tukey's post -hoc test show that zones 1 and 2 have statistically different means of basin slope, basin shape, and hypsometric integral. Zones 2 and 3 have statistically different means of basin slope. Zones 1 and 3 have statistically different means of hypsometrical integral. Overall, the means of most parameters including Ba, Bs, CI, Smd, DBO are fairly similar in zones 1 and 3 (plunges).

Limb results

Table 3 shows the morphometric parameters associated with drainage networks and the mean values of the morphometric indices related to the drainage basins for the southern and northern limbs of the anticline. The northern limb is characterized by steeper slopes, depicting more elongated and younger basins (higher S, Bs and HI values) with higher values of drainage basin orientation, compared to the southern limb. The values of drainage density, drainage frequency, and 1st order drainage density are also higher in the northern limb. The southern limb is characterized by larger basins, with higher values of asymmetry factor, crescentness index and sinuosity of main channel.

Box plots of the morphometric parameters in the northern and southern limbs of the Handun anticline are given in Fig. 10. The median values of Ba, AF, CI, and Smd are higher in the southern limb than northern one. The median values of S, Bs, Hi, and DBO are higher in the northern limb compared to the southern one. According to the t-test values (Table 4), there is statistically significant difference between mean of basin area in the northern and southern limbs.

Regression analysis

To evaluate the quality of the relationship between the resulting morphometric parameters, linear regressions were performed. Pearson's correlation coefficient (r) and confidence levels of p = 0.01 and p = 0.05 for different parameters are given in Table 6. Drainage basin orientation is strongly correlated with crescentness index, sinuosity of main channel, and basin area; so that the values of CI, Smd, and Ba increase with DBO. Basin area (Ba) is strongly positively correlated with the S, AF, CI, Smd, and DBO indexes, whereas it is strongly negatively correlated with Bs and HI (Table 6). Topographic slope (S) of basins has a strong positive correlation with CI, and a strong negative correlation with Bs. Basin shape (Bs) is strongly negatively correlated with CI and Smd. The crescentnes index (CI) of basins is strongly positively correlated with Smd and DBO.

Discussion

The Bandar Abbas syntaxis, as a transitional zone between the Zagros belt, the Makran convergence zone, and the Oman Mountains, hosts numerous salt diapirs. Lateral and vertical fold growth as well as the geodynamic history of a salt diapir in the central part of Handun anticline is likely to have strongly controlled the fold shape and the fluvial landscape morphometric properties. Geomorphic evidence, including a decrease in the fold limb dip towards the west and east (Fig. 2), a decrease in relief of the topographic profile along the fold crest towards the west and east (Fig.4), a decrease in the sinuosity of the anticline drainage divide (Sad) from the core of the anticline towards west and east (Table 1), development of fan-shaped and asymmetric forked drainage patterns in the western and eastern fold plunge regions (Fig. 6), and formation of three wind gaps around the western plunge of the anticline (Fig. 3) collectively demonstrate lateral propagation of the Handun anticline towards the west and east. In accordance with criteria of Hetzel (Hetzel et al., 2004; Keller and DeVecchio, 2022), a decrease in wind gap elevation towards west (Fig. 3) implies lateral growth of the Handun anticline towards the west. The decrease in elevations of the bases of the wind gaps from east to west (Fig. 3), and the presence of a water gap flowing around the western nose of the fold collectively reinforce the westwards lateral propagation of the Handun anticline. As Fig. 5 shows, field geomorphological evidence demonstrates that wind gap 3 has been recently abandoned. Development of the fan-shaped and asymmetric forked drainage network on the fold plunges, especially that of the western one, is further strong evidence for lateral anticline growth (Fig. 6). Most of the asymmetric forked drainage networks are observed in the southern limb of the western zone, where the tributary headwaters (often 1st order drainages) have been curved towards the central parts of the anticline. The development of triangular facets and wine-glass valleys in the central zone (Fig. 5), and the lack of these features in the western and eastern zones, depicts a youthful topography with less erosion, also implying lateral fold growth.

Results show that the older and high-amplitude segment of the fold (central zone) is characterized by larger and relatively circular basins, and a higher sinuosity of its anticlinal ridge drainage divide (Sad), implying dominance of lateral and headward erosion. In contrast, the smaller and highly elongated basins in the plunge areas (western and eastern zone) depict less eroded and younger topography. Data shows that the western and eastern plunges have lower values of topographic slope, indicating a more youthful topography due to the less marked amplitudes of these zones, compared with central zone with its high-amplitude and steep-sloped topography. It is expected that values of the hypsometric integral would be lower in the central zone of anticline compared to the plunges. Results show that the mean HI is higher in the western zone than that of the central zone, whereas the mean HI is lower in the eastern zone than that of the central zone (Table 1). This confirms a more youthful topography for the western fold plunge and active lateral growth towards the west. The absolute values of the asymmetry factor increase from the eastern zone towards the western zone. It is expected that basins formed in the western and eastern zones will be tilted towards the fold tips, because the topographic slopes and the dip of the strata are generally towards the fold noses. Nevertheless, a regular trend in the direction of basin tilting is lacking (Fig. 8). Bahrami et al. (2020) attributed this lack of regular trend in the direction of basin tilting in the Gorm anticline (Fars region), to the curvature or crescentness of the drainage basins and their main channels. They argued that in the initial stages of the fold growth, the main drainage of elongated basins migrates towards the fold tip. With increasing lateral growth of the fold, the headwater areas of the basins tend to be curved towards the center of the fold and, hence, a crescent-shaped basin can form. In this stage, the upstream segment of the main channel migrates perpendicular to the hinge, towards adjacent syncline, and hence tends to decrease the drainage area on the right hand (facing downstream) of the trunk stream. Therefore, the upstream and downstream segments of the main drainage of a crescent-shaped basin affect the asymmetry factor in a reverse manner, so that the downstream part of the trunk channel tends to increase the drainage area on the right hand of the trunk stream, whereas the upstream part of main channel tends to decrease it (see Fig. 14 in Bahrami et al., 2020).

Results show that the southern limb is characterized by larger basins, with higher values of asymmetry factor, crescentness index and sinuosity of the main channels (Table 3), suggesting a higher lateral erosion of this limb. In contrast, steeper slopes, highly elongated and younger basins (higher, Bs, Bs, and HI values) with higher values of drainage basin orientation in the northern limb reflect a more youthful topography and lower erosion.

Note that values of the crescentness index and sinuosity of the main channels are higher in the central zone compared to the western and eastern fold plunge zones (Table 1). Generally, in the older and more uplifted segment of the central zone, the main drainages of the basins are more sinuous due to the lateral erosion of these basins. Also, due to this lateral erosion, basins are more crescent-shaped in the central zone, whereas younger basins of the western and eastern zones with lower erosion have lower values of CI and Smd.

Although different geomorphological evidence of lateral and vertical growth of folds have been proposed (Keller et al., 1999; Azor et al., 2002; Ramsey et al., 2008; Bretis et al., 2011; Bahrami, 2013; Collignon et al., 2016; Bahrami et al., 2020), all of the geomorphic evidence associated with fold growth may not be evident from a given fold because of erosion. Hence, new geomorphic indicators are required to detect lateral fold growth. In this study, a new morphometric index, drainage basin orientation (DBO), was calculated for 57 basins in three tectonic zones of anticline and its relation with other morphometric parameters were evaluated. Results show that drainage basin orientation is strongly correlated with crescentness index, basin area, and sinuosity of main drainage, implying that the value of drainage basin orientation is higher in larger and more crescent-shaped basins with more sinuous main drainage (Table 6). The mean values of DBO, Ba, CI, are higher in the central zone, compared to the western and eastern zones, suggesting that more eroded central zone is marked by the larger and more crescent-shaped basins with more sinuous main drainages. Although the mean value of drainage basin orientation is higher in the central zone, the mean DBO is also high in the western and eastern plunges. Overall, the high values of DBO in the Handun anticline can be explained as follows:

(1) The main reason for increased drainage basin orientation in the fold plunge zones (western and eastern zones) is the presence of an asymmetric forked drainage pattern or curved drainages. In the early stages of fold growth, drainages are either not curved or are less curved, whereas with progressive lateral growth of the fold over time, headwater tributaries become curved towards the core of the anticline, and hence a crescent-shaped basin can develop on the fold plunges (Fig. 11). The general trends of the main channel of these crescent-shaped basins that are often oblique to the fold axis, have resulted in the increased values of drainage basin orientation (DBO) in the western and eastern zones. This situation is in accordance with the finding of Bahrami et al.

(2020) study, demonstrated the development of crescent-shaped basins in the pre-nose segment of Gorm anticline in Fars area, where the upstream parts of basins have been curved towards the central part of the anticline.

(2) Faults and fractures can also affect the trends of the DBO. Major faults of the Zagros Simply Folded Belt include belt-parallel faults and belt-oblique faults (Sepehr and Cosgrove, 2007). Aside from major faults, there are numerous fractures with different trends formed on the folds. Although precise information about the kinematics between the folds and faults are not available for the study area anticline, the findings of some studies from different parts of the Zagros have shown that minor faults and fracture systems are related to either folds, or major basement faults (such as Sarvestan, Bala Rud, Kazerun, Izeh, and Anaran faults) with strike-slip deformation (Mobasher and Babaie, 2008; Tavani et al., 2014; Joudaki et al., 2016). The fold-related fractures are the axial (FA), cross-axial (FC), and two oblique (FO1 and FO2) fracture sets (Mobasher and Babaie, 2008; Joudaki et al., 2016). Fractures associated with major basement faults are five sets (including: synthetic Riedel shear fractures (R); antithetic Riedel shear fractures (R ′); synthetic P-shear fractures; Y-shear fractures, parallel to the main strike-slip fault; and extensional T-set fractures, parallel to the principal shortening direction (Z) (Mobasher and Babaie). Among these fractures, oblique fractures as well as extensional fractures oriented parallel to the anticline axes have exerted a major control in the increase of drainage basin orientation. For example, the main drainages of basins 10, 16, 18, and 19, with high DBO values (Table 5) coincide with oblique fractures in the western zone (Fig. 12). Also, with progressive growth of the anticline over time, oblique faults or fractures can join to the normal faults or fractures oriented parallel to the fold axis (Fig. 13), and thereby curved drainages with high DBO values are formed. Overall, Numerous faults and fractures oriented oblique

and parallel to the fold axis in some anticlines of Zagros belt such as Anaran (Joudaki et al., 2016), Kuhe-Asmari (McQuillan, 1973; Carminati et al., 2013), Bankol (Bahrami, 2022), Sim (Carminati et al., 2013), Kabir-Kuh (Pireh et al., 2006), Bangestan (Tavani et al., 2011), Dil, Khami, and Sulak (Ahmadhadi et al., 2008) anticlines have developed. These faults and major fractures play an important role in the orientation of drainages and their basins on the limbs of folds.

(3) The salt diapir located in the core of the fold also controls the drainage configuration and hence drainage basin orientation in the central zone. In maturely eroded domes such as the study area one, where curved outcrops of alternating resistant/weak sedimentary layers are developed around the salt diapir, a ridge (in resistant rocks) and valley (in soft layers) topography is formed. In this semi-annular drainage pattern, the main drainages are arranged into a circular pattern with subsidiary drainages configured at right angles to them. As Fig. 14 shows, this drainage pattern in the southern part of salt diapir in the central zone has developed some curved main drainages resulting in the increase of the values of drainage basin orientation (i.e., basins 45 with high DBO value).

(4) The tectonic geomorphic history of the basins also controls the value of drainage basin orientation. Although the value of DBO is increasing from noses towards the fold central part, some basins (52 and 55) around the fold nose have higher values of DBO and CI. The positions of basins 52 and 55 coincide with wind gaps 1 and 2 in the western plunge (Figs. 3 and 8), where the abandonment of river channels has resulted in the formation of dry valleys that are now crescent-shaped basins in which their main channels are oriented oblique to the fold axis. Specifically, basin 52 (coincides with wind gap 1) with high value of drainage basin orientation (43°), and crescentness index (1.31), and highest value of sinuosity of main channel (2.57) amongst all basins,

comprises an abandoned deeply entrenched, meandering channel. This shows that tectonic geomorphic history of basins can exert an important role in the present day orientation and other morphometric properties of channels and basins.

Comparison of the morphometric properties of drainage networks across the three tectonic zones shows that values of drainage density (Dd), 1st order drainage density (Dd1), and drainage frequency (Df) are higher in the plunges (western and eastern zone) compared to the central zone (Table 1). Higher values of the1st order drainage density in the plunges especially the western plunge shows younger and less-developed drainage networks in these areas. Results also shows that values of Dd, Dd1 and Df are higher in the less-eroded and steeply-sloped northern limb, compared with highly-eroded southern limb. Hence, results imply that more eroded parts of the anticline (central zone and southern limb) have lower drainage density and frequency, compared to the younger and less-eroded segments of the Handun anticline.

Fig. 14 shows the spatial variation in drainage pattern in different parts of the anticline. A fan-shaped drainage pattern is developed around the ends of the anticline noses. A dendritic drainage pattern is observed in the central zone. Parallel and curved parallel drainage patterns are developed in the western and eastern zones. Radial drainage pattern is observed in the central zone. An asymmetric forked drainage pattern is developed on the southern limb of the western zone, especially in the pre-nose area. A semi-annular drainage pattern is developed around the salt diapir in the core of anticline (Basin 44) (Fig. 14).

The effect of lithology should also be considered as a secondary factor in decreasing values of Hypsometric integral and basin shape. Results show that nearly all basins (except basins 37, 43 and 45) are dominated by strong bedrocks. Basins 37 and 45 in the central zone are characterized by weak strength rocks, as <50% of these basins are composed of rock type 1 (strong). Basin 43 in the eastern zone is characterized by intermediate strength rocks, as 50 to

70% of these basins are composed of rock type 1. Hence, the lithological effect should also be considered in decreasing values of HI and Bs indexes in the central and eastern zones, where the exposure of some soft rocks has facilitated the lateral and vertical erosion and hence decreasing HI and Bs indexes.

Conclusion

Drainage basins and their networks formed on an actively growing anticline are affected by the interaction of surface processes and active tectonics affecting the folds. The Handun anticline in the Bandar Abass region, as part of the hinterland or syntaxis, is a transitional area between three geological zones of the Zagros collisional belt to the NW, the Makran accretionary prism to the east, and the Oman Mountains to the SE. The salt-cored Handun anticline with numerous drainage basins, often oriented oblique to the fold axis, was selected to analyze the effect of active tectonics on the drainage basin orientation and other morphometric parameters of basins and their networks. Data show that drainage basin orientation is strongly correlated with crescentness index, basin area, and sinuosity of main drainage, implying that the value of drainage basin orientation is higher in larger and more crescent-shaped basins with more sinuous main drainage. The mean values of drainage basin orientation, basin area, crescentness index are higher in the central zone, compared to the western and eastern zones, suggesting that more eroded central zone is marked by the larger and more crescent-shaped basins with more sinuous main drainages. Southern flank of anticline is characterized by larger basins, with higher values of asymmetry factor, crescentness index and sinuosity of main channel, implying the higher lateral erosion, while steeper slopes, highly elongated and younger basins (higher, Bs, Bs, and HI values) with higher value of drainage basin orientation in the northern limb imply the youthful of topography and lower erosion.

It is worth noting that although the values of drainage basin orientation are higher in the central zone, the mean DBO is also high in the western and eastern plunges. The high DBO value can be attributed to four parameters: (1) the presence of asymmetric forked drainage pattern or curved drainages, which their general trends are often oblique to the fold axis, resulted in the increased values of drainage basin orientation in the western and eastern zones; (2) the trend of faults and fractures, especially oblique fractures oriented parallel to the anticline axis that exert strong control in the increase of drainage basin orientation; (3) the semi-annular drainage pattern formed around the salt diapir located in the core of the fold, in which main drainages are arranged in a circular pattern with subsidiary drainages lying at right angles to them, resulting in the increased values of drainage basin orientation; and (4) tectonic geomorphic history of basins, so that some basins (52 and 55), with higher values of DBO, coincide with wind gaps 1 and 2 in the western plunge, where the abandonment of river channels has caused the formation of dry valleys that are now crescent-shape basins in which their main channels are oriented oblique to the fold axis.

Overall, a decrease in the values of sinuosity of anticline divide, drainage basin orientation, and crescentness index from the core of anticline towards west and east, development of fan-shaped and asymmetric forked drainage patterns in the western and eastern plunge, formation of three wind gaps around the western plunge of the anticline, imply the lateral propagation of Handun anticline towards west and east.

Declaration of Competing Interest

The author declare that he has no known competing financial interests or personal relationships that could have appeared to influence the work reported in this paper.

References

Adams, J., 1980. Active tilting of the United States midcontinent: geodetic and geomorphic evidence. Geology 8, 442-446.

Adeoti, B., Webb., A.A.G., 2022. Geomorphology of contractional salt tectonics along the Kuqa fold-thrust belt, northwestern China: Testing pre-kinematic diapir versus source-fed thrust and detachment fold models. Journal of Structural Geology 161, 104638.

Altin, T.b., Altin, B.N., 2011. Development and morphometry of drainage network in volcanic terrain, CentralAnatolia, Turkey. Geomorphology 125, 485–503.

Ambraseys, N.N., Melville, C.P., 1982. A history of Persian Earthquakes, Cambridge Earth Science Series, Cambridge University Press, London.

Azor, A., Keller, E.A., Yeats, R.S., 2002. Geomorphic indicators of active fold growth: South Mountain–Oak Ridge anticline, Ventura basin, southern California. Geol. Soc. Am. Bull. 114 (6), 745–753.

Bahrami, S., 2013. Analyzing the drainage system anomaly of Zagros basins: implications for active tectonics. Tectonophysics 608, 914–928.

Bahrami, S., 2022. Analysis of confluence angle of drainages and its relation to morphometric properties of drainage basins in the Zagros Simply Folded Belt, Iran. Geomorphology 400, 108091.

Bahrami, S., Capolongo, D., Rahdan Mofrad, M., 2020. Morphometry of drainage basins and stream networks as an indicator of active fold growth (Gorm anticline, Fars Province, Iran). Geomorphology 355, 107086.

Berberian, M., 1995. Master ‘blind’ thrust faults hidden under the Zagros folds: active basement tectonics and surface morphotextonics. Tectonophysics 241, 193–224.

Berberian, M., 2014. Earthquakes and Coseismic Surface Faulting on the Iranian Plateau; A Historical, Social, and Physical Approach (Developments in Earth Surface Processes 17). Elsevier, Amsterdam, Netherlands (776 pp.)

Berberian, M., Tchalenko, J.S., 1976. Earthquakes of Bandar Abbas-Hadji-Abad region, Zagros (Iran). In: Berberian, M. (Ed.), Contribution to the Seismotectonics of Iran, Part II. vol. 39. Geol. Surv. Iran, pp. 371–396.

Berberian, M., Papastamatiou, D., Qoraishi, M., 1977. Khurgu (north Bandar Abbas-Iran) earthquake of March 21, 1977: a preliminary field report and a seismotectonic discussion. In: Berberian, M. (Ed.), Contribution to the Seismotectonics of Iran, Part III. Geol. Min. Surv. Iran, vol. 40, pp. 7–50.

Bishop, M., Shroder, J., Bonk, R., Olsenholler, J., 2002. Geomorphic Change in High Mountains: A Western Himalayan Perspective. Global Planetary Change 32, 311-329.

Bretis, B., Bartl, N., Grasemann, B., 2011. Lateral fold growth and linkage in the Zagros fold and thrust belt (Kurdistan, NE Iraq). Basin Res. 23, 615–630.

Castelltort, S., Goren, L., Willett, S.D., Champagnac, J.D., Herman, F., Braun, J., 2012. River drainage patterns in the New Zealand Alps 384 primarily controlled by plate tectonic strain. Nature Geoscience 5 (10), 744–8

Collignon, M., Fernandez, N., Kaus, B.J.P., 2015. Influence of surface processes and initial topography on lateral fold growth and fold linkage mode. Tectonics 34. https://doi. org/10.1002/2015TC003843.

Collignon, M., Yamato, P., Castelltort, S., Kaus, B.J.P., 2016. Modeling of wind gap formation and development of sedimentary basins during fold growth: application to the Zagros Fold Belt, Iran. Earth Surf. Process. Landf. 41, 1521–1535.

Colman-Sadd, S.P., 1978. Fold development in Zagros simply folded belt, southwest Iran. Am. Assoc. Pet. Geol. Bull. 62, 984–1003.

Delcaillau, B., Carozza, J.M., Laville, E., 2006. Recent fold growth and drainage development: the Janauri and Chandigarh anticlines in the Siwalik foothills, northwest India. Geomorphology 76, 241–256.

Delcaillau, B., Deffontaines, B., Angelier, J., Déramond, J., Floissac, L., Souquet, P., Chu, H.T., 1998. Morphotectonic evidence from lateral propagation of an activefrontal fold; the Pakuashan anticline, foothills of Taiwan. Geomorphology 24, 263–290.

Devi, R.K.M., Bhakuni, S.S., Bora, P.K., 2011. Tectonic implication of drainage set-up in the Sub-Himalaya: a case study of Papumpare district, Arunachal Himalaya, India. Geomorphology 127, 14–31.

El Hamdouni, R., Irigaray, C., Fernndez, T., Chacon, J., Keller, E.A., 2008. Assessment of relative active tectonics, southwest border of the Sierra Nevada (Southern Spain). Geomorphology 96, 150–173.

Faghih, A., Nourbakhsh, A., 2014. Appraisal of relative tectonic activity along the Kazerun Fault Zone, Zagros Mountains, Iran: insight from spatial analysis of geomorphic indices. Geol. J. https://doi.org/10.1002/gj.2597.

Faridi, P., Rezaee, P., Piryaei, A., Masoodi, Masoodi, Masoodi, M., 2021. Halokinetic sequences as indicators of Cenozoic diapiric growth: The Handun Salt Diapir (SE Zagros, Bandar Abbas). Geopersia 11(2), 299-317.

García-Delgado, H., Velandia, F., 2020. Tectonic geomorphology of the Serranía de San Lucas Central Cordillera): Regional implications for active tectonics and drainage rearrangement in the Northern Andes. Geomorphology 349, 106914.

Gharabeili, G.R., 2005. 1:100000 Geologic Map of Fin (Sheet 20870E). National Iranian Oil Company.

Ginés, J., Edwards, R., Lohr, T., Larkin, H. and Holley, R., 2019. Remote sensing applications in the Fars Region of the Zagros Mountains of Iran. Geological Society, London, Special Publications, 490, 417-444.

Hare, P.W., Gardner, T.W., 1985. Geomorphic indicators of vertical neotectonism along converging plate margins, Nicoya Peninsula, Costa Rica. In: Morisawa, M., Hack, J.T. (Eds.), Tectonic Geomorphology. Proceedings of the 15th Annual Binghamton Geomorphology Symposium. Allen and Unwin, Boston, MA, pp. 123–134.

Harlin, J.M., 1978. Statistical moments of the hypsometric curve and its density function. Journal of the International Association for Mathematical Geology, 10(1), 59–72

He, C., Rao, G., Yang, R., Hu, J., Yao, Q., Yang, C-J., 2019. Divide migration in response to asymmetric uplift: Insights from the Wula Shan horst, North China. Geomorphology 339, 44–57.

Hetzel, R., Tao, M., Niedernann, S., Strecker, M., Ivy-Ochs, S., Kubik, P., Gao, B., 2004. Implications of the fault scaling law for the growth of topography: Mountain ranges in the broken foreland of north-East Tibet. Terra Nova 16 (3), 157–162.

Horton, R.E., 1932. Drainage basin characteristics. Trans. Am. Geophys. Union 13, 350–361.

ITC, 2007. Integrated Land and Water Information System (ILWIS). ITC, The Netherlands. http://www.itc.nl/ ilwis33.asp.

Jahani, S., Callot, J.P., Frizon de Lamotte, D., Letouzey, J., Leturmy, P., 2007. The salt diapirs of the eastern Fars province (Zagros, Iran): A brief outline of their past and present, in: Thrust Belt and Foreland Basin, edited by O. Lacombe et al., pp. 289 – 308, Springer, Berlin.

Jahani, S., Callot, J. P., Letouzey, J., Frizon de Lamotte, D., 2009. The eastern termination of the Zagros Fold and Thrust Belt, Iran: Structures, evolution, and relationships between salt plugs, folding, and faulting. Tectonics 28(6), C6004. https://doi.org/10.1029/2008TC002418.

Jackson, J., Van Dissen, R., Berryman K., 1998. Tilting of active folds and faults in the Manawatu region, New Zealand: evidence from surface drainage patterns. New Zealand Journal of Geology and Geophysics 41, 377–385.

Joshi, P.N., Maurya, D.M., Chamyal, L.S., 2013. Morphotectonic segmentation and spatial variability of neotectonic activity along the Narmada–Son Fault, Western India: Remote sensing and GIS analysis. Geomorphology 180-181, 292-306.

Joudaki, M., Farzipour-Saein, A., Nilfouroushan, F., 2016. Kinematics and surface fracture pattern of the Anaran basement fault zone in NW of the Zagros fold-thrust belt. Int. J. Earth Sci. 105 (3), 869–883.

Keller, E.A., DeVecchio, D.E., 2022. Tectonic geomorphology of active folding and development of transverse drainages. In: Treatise on Geomorphology (second edition). Elsevier Inc., pp. 477–494.

Keller, E.A., Gurrola, L., Tierney, T.E., 1999. Geomorphic criteria to determine direction of lateral propagation of reverse faulting and folding. Geology 27, 515–518.

Keller, E.A., Pinter, N., 2002. Active Tectonics: Earthquakes, Uplift, and Landscape (Second Edition): Englewood Cliffs. Prentice Hall, New Jersey (362 pp.).

Krystopowicz, N.J., Schoenbohm, L.M., Rimando, J., Brocard, G., Rojay, B., 2020. Tectonic geomorphology and Plio-Quaternary structural evolution of the Tuzgölü fault zone, Turkey: Implications for deformation in the interior of the Central Anatolian Plateau. Geosphere 16 (5), 1107–1124.

Langbein, W.B., 1947. Topographic characteristics of drainage basins. U.S. Geol. Surv., Water Supply Pap., 968C, 125-157.

Lees, G.M., Falcon, N.L., 1952. The geographical history of the Mesopotamian Plains. The Geographical Journal 118, 24–39.

Liffner, J.W., Hewa, G.A., Peel, M.C., 2018. The sensitivity of catchment hypsometry and hypsometric properties to DEM resolution and polynomial order. Geomorphology 309, 112–120.

Machuca, S., García-Delgado, H., Velandia, F., 2021. Studying active fault-related folding on tectonically inverted orogens: a case study at the Yariguíes Range in the Colombian Northern Andes. Geomorphology 375, 107515.

Melosh, B.L., Keller, E.A., 2013. Effects of active folding and reverse faulting on stream channel evolution, Santa Barbara Fold Belt, California. Geomorphology 186, 119–135.

Mobasher, K., Babaie, H.a., 2008. Kinematic significance of fold- and fault-related fracture systems in the Zagros mountains, southern Iran. Tectonophysics 451, 156–169.

Molinaro, M., Guezou, J.C., P. Leturmy, P., Eshraghi, S.A., de Lamotte, D.F., 2004. The origin of changes in structural style across the Bandar Abbas syntaxis, SE Zagros (Iran), Mar. Pet. Geol. 21, 735 – 752.

Molinaro, M., Leturmy, P., Guezou, J. C., de Lamotte, D. F., Eshraghi, S. A., 2005. The structure and kinematics of the southeastern Zagros fold thrust belt, Iran: From thin skinned to thick skinned tectonics. Tectonics, 24(3), TC3007.

Özkaymak, Ç., Sözbilir, H., 2012., Tectonic geomorphology of the Spildağı High Ranges, western Anatolia. Geomorphology 173–174, 128–140.

Pavano, F., Catalano, S., Romagnoli, G., Tortorici, G., 2018. Hypsometry and relief analysis of the southern termination of the Calabrian arc, NE-Sicily (southern Italy). Geomorphology 304, 74–88.

Peréz-Peña, J.V., Azor, A., Azañon, J.M., Keller, E.A., 2010. Active tectonics in the Sierra Nevada (Betic Cordillera, SE Spain): insights from geomorphic indexes and drainage pattern analysis. Geomorphology 119, 74–87.

Peyrowan, H.R., Shariatjafari, M., 2013. Presentation of a comprehensive method for determining erodibility rate of rock units with a review on Iranian geology. J. Watershed Eng. Manag. 5 (3), 199–213 (in Persian).

Ramírez-Herrera, M.T., 1998. Geomorphic assessment of active tectonics in the Acambay Graben, Mexican volcanic belt. Earth Surf. Process. Landf. 23, 317–332.

Ramsey, L.A., Walker, R.T., Jackson, J., 2007. Geomorphic constraints on the active tectonics of southern Taiwan. Geophys. J. Int. 170, 1357–1372.

Ramsey, L.A., Walker, R.T., Jackson, J., 2008. Fold evolution and drainage development in the Zagros mountains of Fars province, SE Iran. Basin Res. 20, 23–48.

Ribolini, A., Spagnolo, M., 2008. Drainage network geometry versus tectonics in the Argentera Massif (French–Italian Alps). Geomorphology 93, 253–266.

Rowan, M. G., Vendeville, B.C., 2006. Foldbelts with early salt withdrawal and diapirism: Physical model and examples from the northern Gulf of Mexico and the Flinders Ranges, Australia, Mar. Pet. Geol. 23 (9 – 10), 871 – 891.

Różycka, M., Migoń, P., 2021. Morphometric properties of river basins as indicators of relative tectonic activity – Problems of data handling and interpretation. Geomorphology 389, 107807.

Sepehr, M., Cosgrove, J.W., 2004. Structural framework of the Zagros fold-thrust belt, Iran. Mar. Pet. Geol. 21, 829–843.

Sepehr, M., Cosgrove, J.W., 2007. The role of major fault zones in controlling the geometry and spatial organisation of structures in the Zagros Fold-Thrust Belt. In: Ries, A.C., Butler, R.W.H., Graham, R.H. (Eds.), Deformation of the Continental Crust: The Legacy of Mike Coward. 272. Geological Society, London, Special Publications, pp. 419–436.

Sepehr, A., Honarmandnejad, S., 2012. Actual soil erosion risk mapping using modified CORINE method (case study: Jahrom Basin). Geogr. Environ. Hazards 3, 57–72 (in Persian).

Sherkati, S., Molinaro, M., Frizon de Lamotte, D., Letouzey, J., 2005. Detachment folding in the Central and Eastern Zagros fold-belt (Iran): salt mobility, multiple detachments and late basement control. J. Struct. Geol. 27 (9), 1680–1696.

Singh, O., Sarangi, A., Sharma, M.C., 2008. Hypsometric Integral Estimation Methods and its Relevance on Erosion Status of North-Western Lesser Himalayan Watersheds. Water Resources Management 22, 1545-1560.

Stokes, M., Mather, A.E., 2015. Controls on modern tributary-junction alluvial fan occurrence and morphology: high Atlas Mountains, Morocco. Geomorphology 248, 344–362.

Strahler, A.N., 1952. Hypsometric (Area-Altitude) Analysis of Erosional Topography. Geological Society of America Bulletin 63, 1117-1141.

Strahler, A.N., 1957. Quantitative analysis of watershed geomorphology. Trans. Am. Geophys. Union 38, 913–920.

Talebi, A., 2007. 1:100000 Geologic Map of Khoshangan (Sheet 20870E). National Iranian Oil Company.

Tavani, S., Snidero, M., Muñoz, J.A., 2014. Uplift-induced residual strain release and latethrusting extension in the Anaran mountain front anticline, Zagros (Iran). Tectonophysics 636, 257–269.

Wells, S.G., Bullard, T.F., Menges, C.M., Drake, P.G., Karas, P.A., Kelson, K.I., Ritter, J.B., Wesling, J.R., 1988. Regional variations in tectonic geomorphology along a segmented convergent plate boundary, Pacific coast of Costa Rica. Geomorphology 1, 239–265.

Woodbridge, K.P., Pirasteh, S., Parsons, D.R., 2019. Investigating fold-river interactions for major rivers using a scheme of remotely sensed characteristics of river and fold geomorphology. Remote Sens. 11, 2037. https://doi.org/10.3390/rs11172037.

Zámolyi, A., Székely, B., Draganits, E., Timár, G., 2010 Neotectonic control on river sinuosity at the western margin of the Little Hungarian Plain. Geomorphology 122, 231–243.

Zare, M., Amini, H., Yazdi, P., Sesetyan, K., Demircioglu, M.B., Kalafat, D., et al. 2014. Recent developments of the Middle East catalog. J. Seismol. 18(4):749-772.

Zuchiewicz, W., 1998. Quaternary tectonics of the Outer West Carpathians, Poland. Tectonophysics 297, 121–132.

Table captions

Table 1. Mean values of morphometric properties of 57 basins. Basins 1 to 25 and 46 to 57 are in the Western zone, basins 26 to 37 and 44 to 45 are in the central zone, and basins 38 to 43 are in the eastern zone. N is the number of basins.

Table 2. The P-values for ANOVA test (Between Zones), and Tukey's post–hoc test. Marked correlations (bold) are significant at the significance level of $p = 0.05$.

Table 3. Mean values of morphometric parameters associated with drainage networks (Dd, Dd1, and Df), sinuosity of anticline divide (Sad) and the means of the morphometric properties related to the drainage basins (Ba, S, Bs, HI, AF, CI, Smd, and DBO) in the northern and southern limbs of the anticline. N is the number of basins.

Table 4. The t-test results comparing means of variables in Northern limb/Southern limb basins. Marked correlations (bold) are significant at the significance level of $p = 0.05$.

Table 5. Summary of drainage basin and their network parameters.

Table 6. Pearson's correlation matrix for morphometric properties of studied basins.

Figure captions

Fig. 1. Regional study location map and detailed topography of the Handun anticline (red line) based on 12.5 m ALOS DEM data.

Fig. 2. Geological map of the Handun anticline and three geological cross-sections in the western nose (AB), central part (C-D), and eastern nose (E-F). Hs; Hormuz Series (salt, gypsum, shale, sandstone and limestone, and igneous rocks), As-Ja; Asmari-Jahrom (limestone and dolomitic limestone), Rz; Razak (marl, siltstone, sandstone and gypsum), Grm; Guri Member (limestone), Bk; Bakhtyari (conglomerate, sandstone, marl), Qt; Quaternary alluvial terraces and deposits.

Fig. 3. Topographic profile (A-B) showing the wind (W1, W2, and W3) and water gaps developed around the western end of the plunging anticline nose.

Fig. 4. Topographic profiles along the fold crest (AA′), across the width of the fold (BB′, CC′, DD′, and EE′), and parallel to the hinge in the northern and southern limbs (FF′ and GG′),

Fig. 5. Major landforms and processes of the Handun anticline; (a) triangular facets, composed of carbonate rocks of the Guri Member, developed in the steeply-sloped southern limb of the central zone; (b) small rillen-karren developed into carbonate rocks of the Guri Member; (c) dry valley (wind gap 1 [W1 in Fig. 3]) formed in the western plunge of the fold; (d) small dry

valley (wind gap 2 [W2 in Fig. 3]) developed in the western plunge of the fold; (e) recently formed dry valley (wind gap 3 [W3 in Fig. 3]) developed around the western end of anticline nose.

Fig. 6. Drainage map of the Handun anticline and its fold structure zonation.

Fig. 7. Graphical summary of methods used for calculating drainage basin orientation (a), sinuosity of main drainage (Smd), crescentness index (c), and sinuosity of anticline divide (d).

Fig. 8. Map of the 57 drainage basins and their main channel networks with respect to the three zones. Red arrows depict the asymmetry directions of the drainage basins.

Fig. 9. Box plots showing the distribution of Ba (km^2), S (%), Bs, HI, AF, CI, Smd, and DBO in three zones of the study area. Box plots represent 25–75% of values, the caps at the end of the vertical lines represent 10–90% of values and the line in the center of the box shows the median value.

Fig. 10. Box plots showing the distribution of Ba (km^2), S (%), Bs, HI, AF, CI, Smd, and DBO in the northern and southern limbs of the Handun anticline.

Fig. 11. Schematic illustration of the formation of asymmetric forked drainage pattern or curved drainage in a crescent-shaped basin, due to the lateral growth of a fold. With further lateral anticline growth, the general trend of the main channel of the crescent-shaped drainage basin becomes oblique to the fold axis, resulting in an increased value of drainage basin orientation (DBO).

Fig. 12. Oblique fractures oriented oblique to the anticline axis having a major control in the increase of drainage basin orientation in basins 10, 16, 18, and 19.

Fig. 13. Schematic representation of the joining of oblique fault/fracture to the normal fault/fracture oriented parallel to the fold axis. At first stage, a drainage coinciding with an oblique fault/fracture is developed (a). With progressive erosion and growth of the anticline over time (b), the oblique drainage can join to the drainage coinciding with the trace of normal fault/fracture oriented parallel to the fold axis, and thereby a curved drainage with high DBO is formed.

Fig. 14. Dendritic, parallel, curved parallel, asymmetric forked, fan-shaped, radial, and semi-annular drainage patterns developed on the flanks of the Handun anticline.

Table 1

Zone	Ba (km^2)	S (%)	Bs	HI	AF	CI	Smd	DBO	Sad	Dd	Dd1	Df
Western	1.93	23.25	5.34	0.63	15.31	1.09	1.19	22	1.23	5.91	3.32	9.28
Central	4.02	54.81	2.46	0.53	12.48	1.13	1.24	24.36	1.37	4.22	2.73	6.18
Eastern	1.73	31.33	4.58	0.46	5.53	1.04	1.16	13.67	1.03	5.01	3.31	6.93

Table 2

Parameter			Ba	S	Bs	HI	AF	CI	Smd	DBO
ANOVA test (Between Zones)			0.249	**0.000**	**0.000**	**0.000**	**0.011**	0.077	0.677	0.224
Tukey's post -hoc test	Zones to compare	1-2	0.242	**0.000**	**0.000**	**0.01**	0.432	0.275	0.726	0.823
		1-3	0.993	0.082	0.677	**0.000**	**0.009**	0.354	0.955	0.298
		2-3	0.488	**0.000**	0.093	0.162	0.129	0.072	0.733	0.201

Table3

Parameters	**Ba (km^2)**	**S (%)**	**Bs**	**HI**	**AF**	**CI**	**Smd**	**DBO**	**Dd**	**Dd1**	**Df**
Northern limb	1.38	33.33	4.76	0.60	13.52	1.09	1.14	23.51	5.76	3.53	8.63
Southern limb	4.67	28.64	4.10	0.56	13.73	1.11	1.32	17.78	4.89	2.87	7.48

Table 4

	t-test parameters		
Parameters	T	df	Sig (2 tailed)
Ba	-2.103	17.82	**0.050**
S	1.045	55	0.300
Bs	0.947	55	0.334
HI	1.394	55	0.169
AF	-0.096	55	0.924
CI	-1.139	55	0.260
Smd	-2.040	17.903	0.056
DBO	1.603	55	0.115

Table 5

Basin No.	**Ba (km^2)**	**S (%)**	**Bs**	**HI**	**AF (%)**	**CI**	**Smd**	**DBO**
1	0.15	8.54	6.16	0.67	10.66	1.00	1.07	19
2	0.16	10.20	4.81	0.59	26.28	1.01	1.07	23
3	0.17	18.23	3.63	0.51	19.95	1.04	1.14	19
4	0.75	11.37	5.96	0.71	15.76	1.31	1.20	32
5	0.41	20.68	4.87	0.74	18.86	1.02	1.07	12
6	0.16	21.20	9.38	0.60	25.45	1.01	1.04	7
7	0.11	18.87	11.43	0.66	10.54	1.02	1.03	6
8	0.39	18.30	5.38	0.70	13.25	1.03	1.04	18
9	0.37	22.36	5.39	0.55	10.45	1.01	1.07	12
10	0.77	24.54	2.47	0.67	21.66	1.07	1.06	22
11	0.33	19.45	4.70	0.68	18.83	1.01	1.05	13
12	0.24	18.34	6.72	0.71	19.88	1.03	1.06	15
13	0.22	17.37	6.89	0.73	10.91	1.01	1.05	14

14	0.20	18.62	6.73	0.73	7.39	1.04	1.05	21
15	0.59	28.97	3.05	0.57	12.48	1.08	1.14	17
16	1.97	31.10	2.23	0.69	25.08	1.10	1.11	32
17	0.86	18.87	7.82	0.77	15.36	1.09	1.15	27
18	2.37	24.38	6.17	0.54	18.85	1.14	1.24	36
19	2.21	26.66	5.71	0.57	7.61	1.14	1.32	38
20	3.82	22.88	7.48	0.48	7.06	1.14	1.27	41
21	3.11	25.95	5.83	0.55	15.30	1.04	1.15	30
22	6.66	32.91	3.41	0.58	35.23	1.09	1.19	38
23	3.71	34.49	5.12	0.69	17.94	1.15	1.18	32
24	2.16	35.17	8.03	0.65	6.45	1.12	1.18	42
25	3.19	42.91	3.25	0.66	4.87	1.07	1.25	20
26	2.24	49.93	3.85	0.72	9.31	1.10	1.18	20
27	1.05	43.82	4.14	0.62	5.33	1.06	1.11	23
28	1.13	51.64	2.42	0.62	5.53	1.09	1.25	5
29	0.65	50.02	4.09	0.59	11.17	1.07	1.05	27
30	0.66	54.18	2.75	0.50	7.92	1.06	1.04	0
31	1.71	48.05	1.16	0.53	0.81	1.23	1.14	10
32	0.29	42.58	5.24	0.47	5.02	1.07	1.15	26
33	0.66	57.85	1.92	0.57	18.83	1.03	1.25	29
34	0.57	69.27	1.53	0.51	9.15	1.14	1.14	28
35	0.78	66.79	1.41	0.54	16.69	1.34	1.16	38
36	1.04	64.86	1.41	0.43	22.35	1.14	1.11	29
37	4.86	57.79	1.42	0.47	10.47	1.15	1.43	42
38	2.85	42.56	8.94	0.44	4.00	1.06	1.17	45
39	0.42	28.26	2.62	0.45	4.46	1.02	1.11	9
40	0.06	24.63	2.79	0.41	1.46	1.01	1.17	7
41	0.33	23.05	4.03	0.47	16.35	1.01	1.18	6
42	0.92	21.85	3.73	0.51	3.99	1.03	1.10	5
43	5.78	47.65	5.37	0.50	2.94	1.11	1.22	10
44	14.92	52.89	1.65	0.48	26.08	1.13	1.64	18
45	25.74	57.71	1.40	0.43	26.11	1.23	1.79	46
46	4.47	38.01	2.24	0.72	19.88	1.16	1.37	7
47	2.31	38.13	5.39	0.68	6.07	1.07	1.11	3
48	3.38	27.01	3.32	0.73	13.87	1.02	1.09	14
49	2.80	24.12	4.95	0.64	23.31	1.09	1.24	18
50	2.96	23.57	6.94	0.56	4.80	1.18	1.25	27
51	10.52	26.06	1.71	0.41	24.02	1.25	1.37	41
52	5.97	24.01	2.33	0.61	16.70	1.31	2.57	43
53	0.69	20.00	4.87	0.65	16.85	1.05	1.13	13
54	0.73	23.02	3.87	0.68	10.01	1.07	1.11	13
55	2.13	20.75	3.31	0.52	7.85	1.28	1.41	35
56	0.18	13.06	8.21	0.61	17.33	1.02	1.03	12
57	0.25	9.99	7.77	0.52	9.52	1.02	1.04	2
Min	0.06	8.54	1.16	0.41	0.81	1.00	1.03	0.00
Mean	2.42	31.45	4.55	0.59	13.58	1.09	1.20	21.70
Max	25.74	69.27	11.43	0.77	35.23	1.34	2.57	46.00
SD	4.12	15.77	2.35	0.10	7.71	0.09	0.23	12.73

Table 6

Parameters	Ba	S	Bs	HI	AF	CI	Smd	DBO
Ba	1							
S	0.323*	1						
Bs	-0.32*	-0.573**	1					
HI	-0.314*	-0.363	0.305	1				
AF	0.344**	-0.094	-0.160	0.120	1			
CI	0.416**	0.329*	-0.374**	-0.185	0.077	1		
Smd	0.605**	0.177	-0.340**	-0.210	0.159	0.596**	1	
DBO	0.406**	0.226	-0.109	-0.202	0.232	0.593**	0.458**	1

** Significant correlation at the 0.01 level.
* Significant correlation at the 0.05 level.

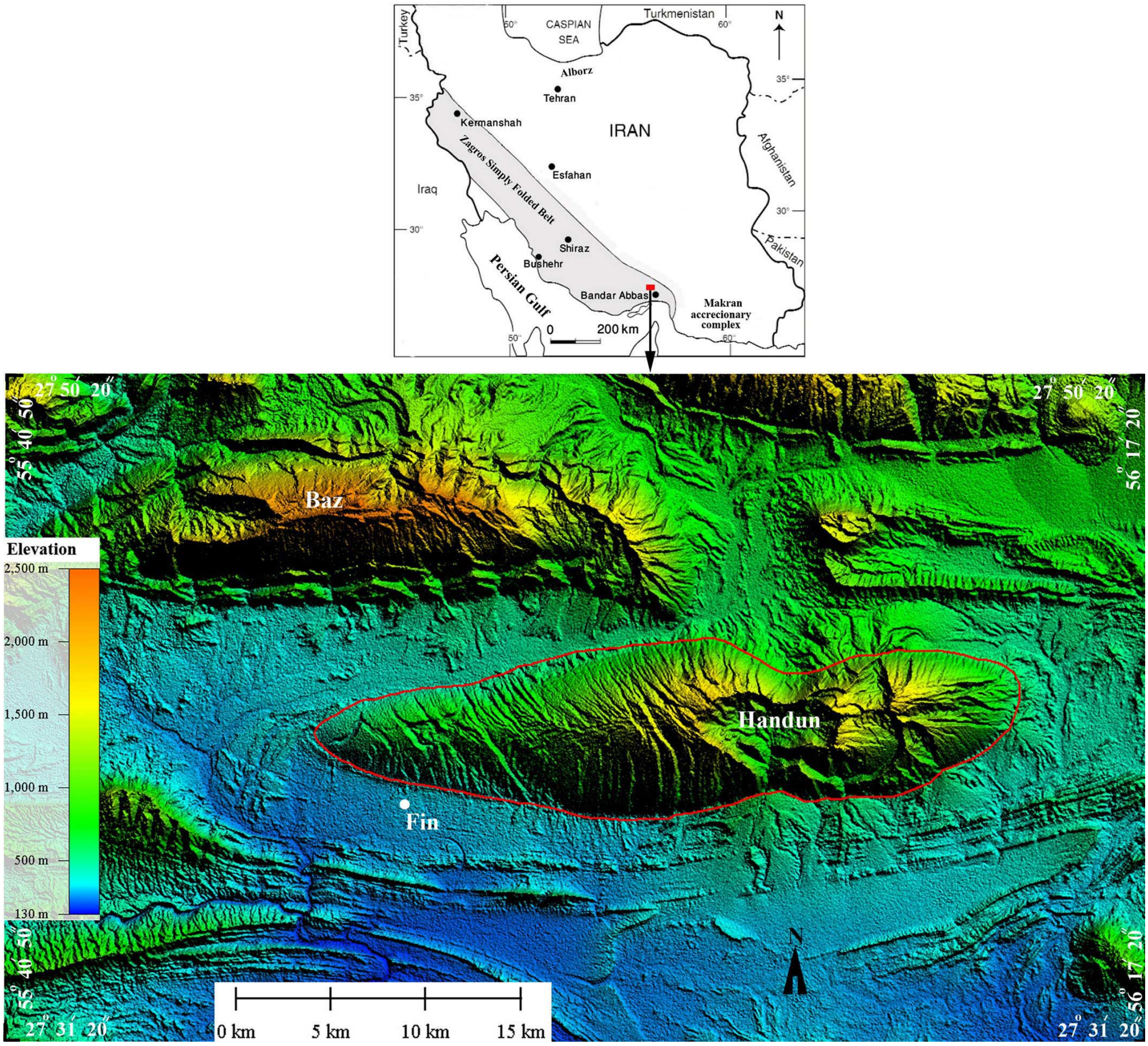
Turkey
CASPIAN SEA
Turkmenistan
N
Alborz
Tehran
Kermanshah
IRAN
Zagros Simply Folded Belt
Esfahan
Afghanistan
Iraq
Shiraz
Bushehr
Persian Gulf
Pakistan
Bandar Abbas
Makran accrecionary complex
0
200 km
Baz
Elevation
2,500 m
2,000 m
1,500 m
1,000 m
500 m
130 m
Handun
Fin
0 km
5 km
10 km
15 km

Fig. 1

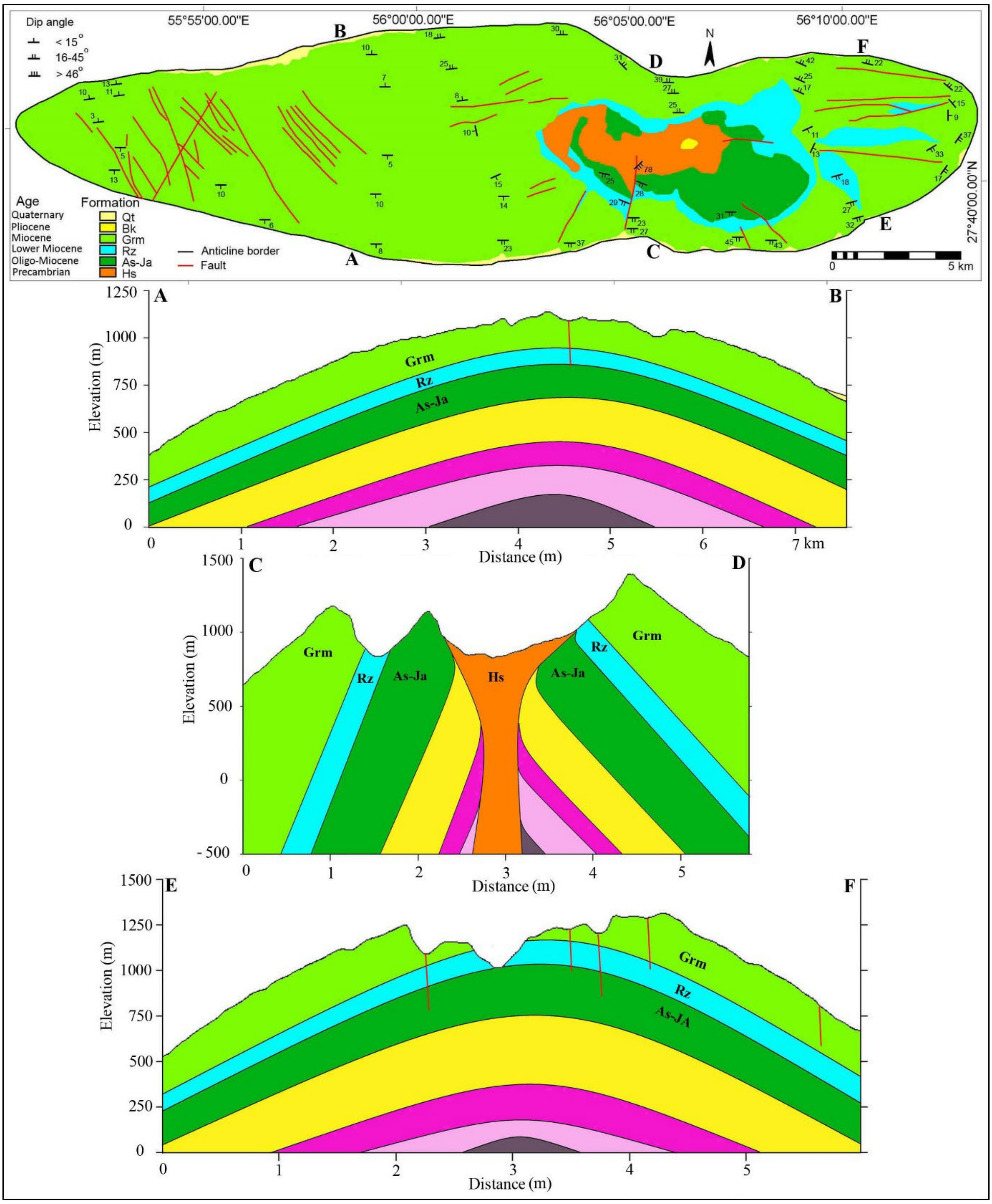

Dip angle
< 15°
16-45°
> 46°
55°55'00.00"E
56°00'00.00"E
56°05'00.00"E
56°10'00.00"E
27°40'00.00"N
N
A
B
C
D
E
F
Age
Formation
Quaternary
Pliocene
Miocene
Lower Miocene
Oligo-Miocene
Precambrian
Qt
Bk
Grm
Rz
As-Ja
Hs
Anticline border
Fault
0
5 km
Elevation (m)
Distance (m)
Grm
Rz
As-Ja
Hs
As-JA
7 km

Fig. 2

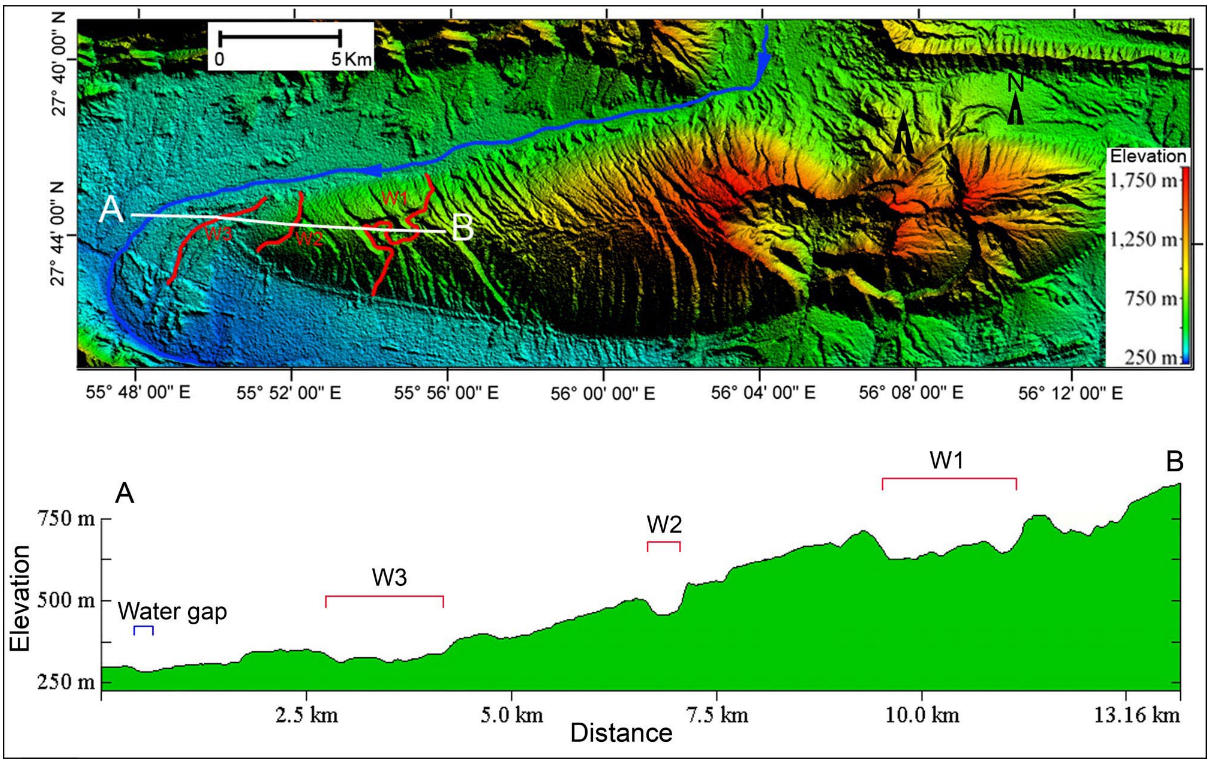

0
5 Km
27° 40' 00" N
27° 44' 00" N
A
B
W1
W2
W3
N
Elevation
1,750 m
1,250 m
750 m
250 m
55° 48' 00" E
55° 52' 00" E
55° 56' 00" E
56° 00' 00" E
56° 04' 00" E
56° 08' 00" E
56° 12' 00" E
A
B
W1
W2
W3
Water gap
750 m
500 m
250 m
Elevation
2.5 km
5.0 km
7.5 km
10.0 km
13.16 km
Distance

Fig. 3

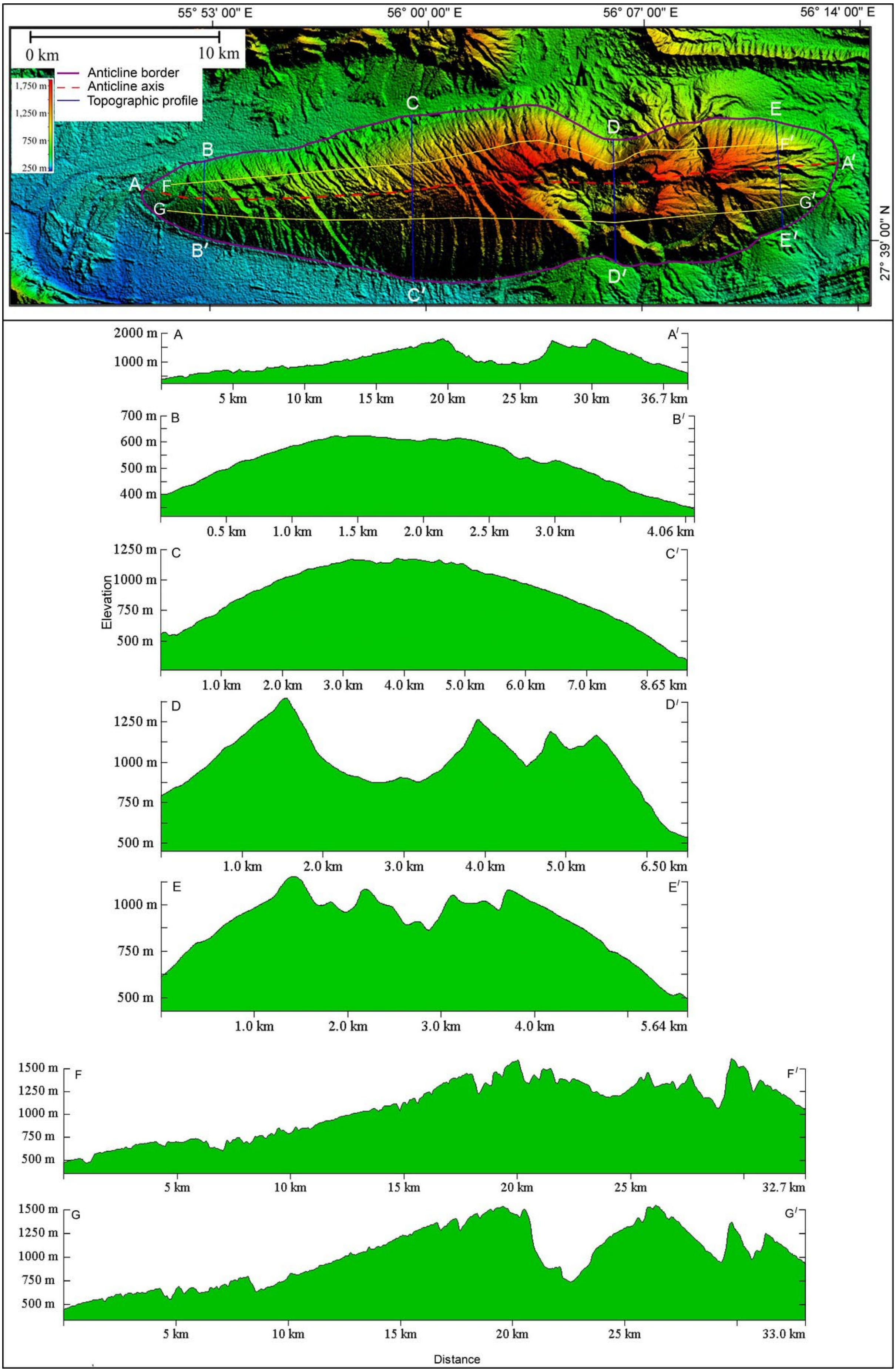
55° 53' 00" E
56° 00' 00" E
56° 07' 00" E
56° 14' 00" E
27° 39' 00" N
0 km
10 km
Anticline border
Anticline axis
Topographic profile
1,750 m
1,250 m
750 m
250 m
N
A
A′
B
B′
C
C′
D
D′
E
E′
F
F′
G
G′
2000 m
1000 m
5 km
10 km
15 km
20 km
25 km
30 km
36.7 km
700 m
600 m
500 m
400 m
0.5 km
1.0 km
1.5 km
2.0 km
2.5 km
3.0 km
4.06 km
1250 m
1000 m
750 m
500 m
Elevation
1.0 km
2.0 km
3.0 km
4.0 km
5.0 km
6.0 km
7.0 km
8.65 km
6.50 km
5.64 km
1500 m
32.7 km
33.0 km
Distance

Fig. 4

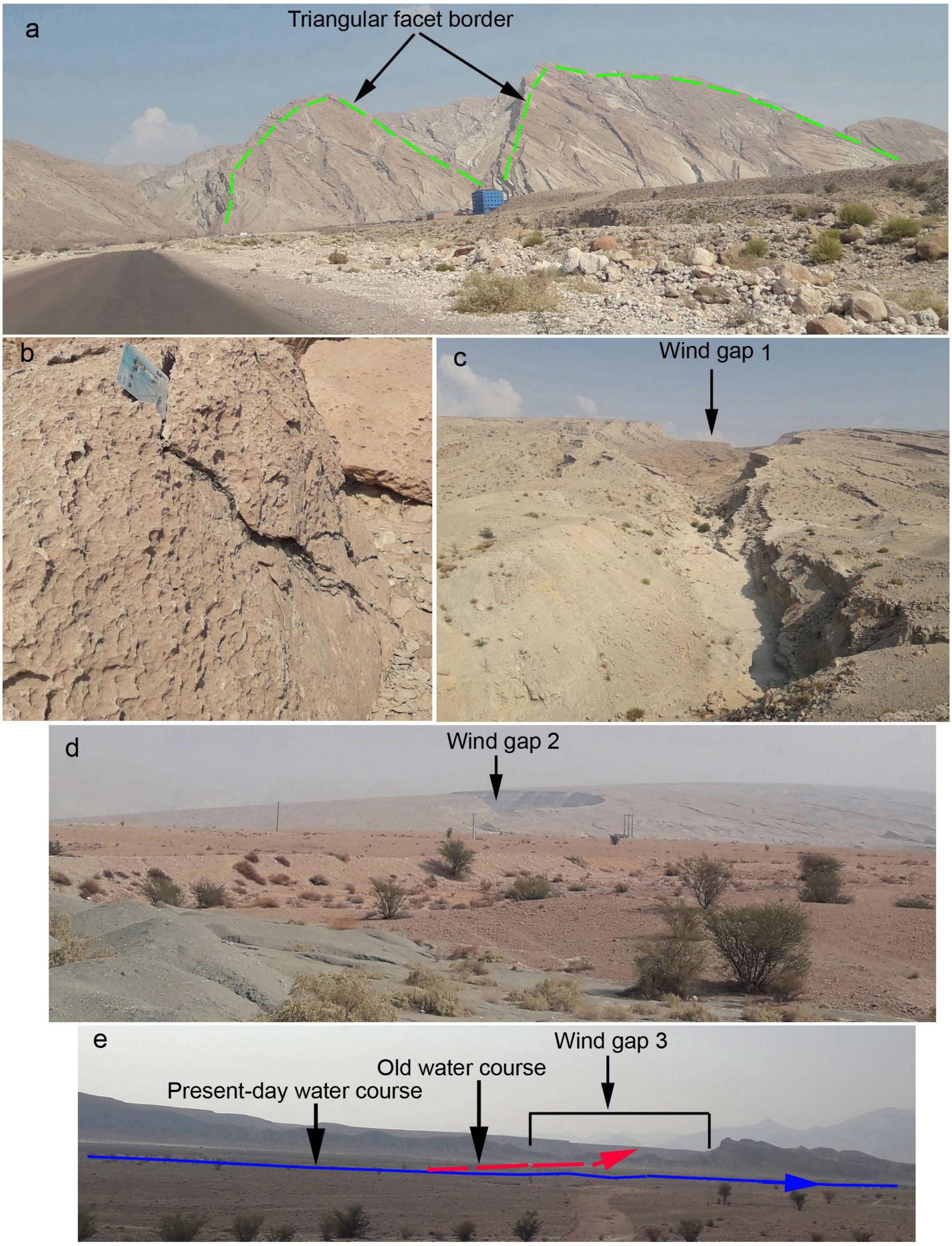
a
Triangular facet border
b
c
Wind gap 1
d
Wind gap 2
e
Wind gap 3
Old water course
Present-day water course

Fig. 5

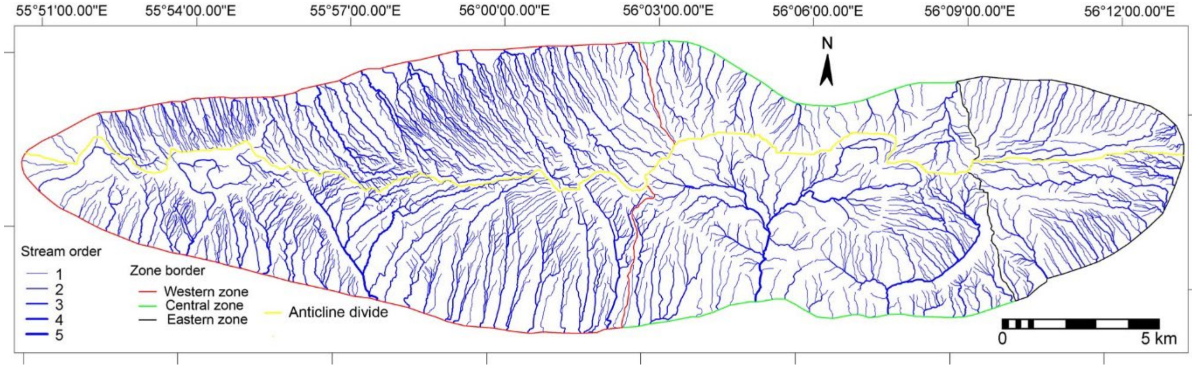
55°51'00.00"E
55°54'00.00"E
55°57'00.00"E
56°00'00.00"E
56°03'00.00"E
56°06'00.00"E
56°09'00.00"E
56°12'00.00"E
27°42'00.00"N
27°39'00.00"N
N
Stream order
1
2
3
4
5
Zone border
Western zone
Central zone
Eastern zone
Anticline divide
0
5 km

Fig. 6

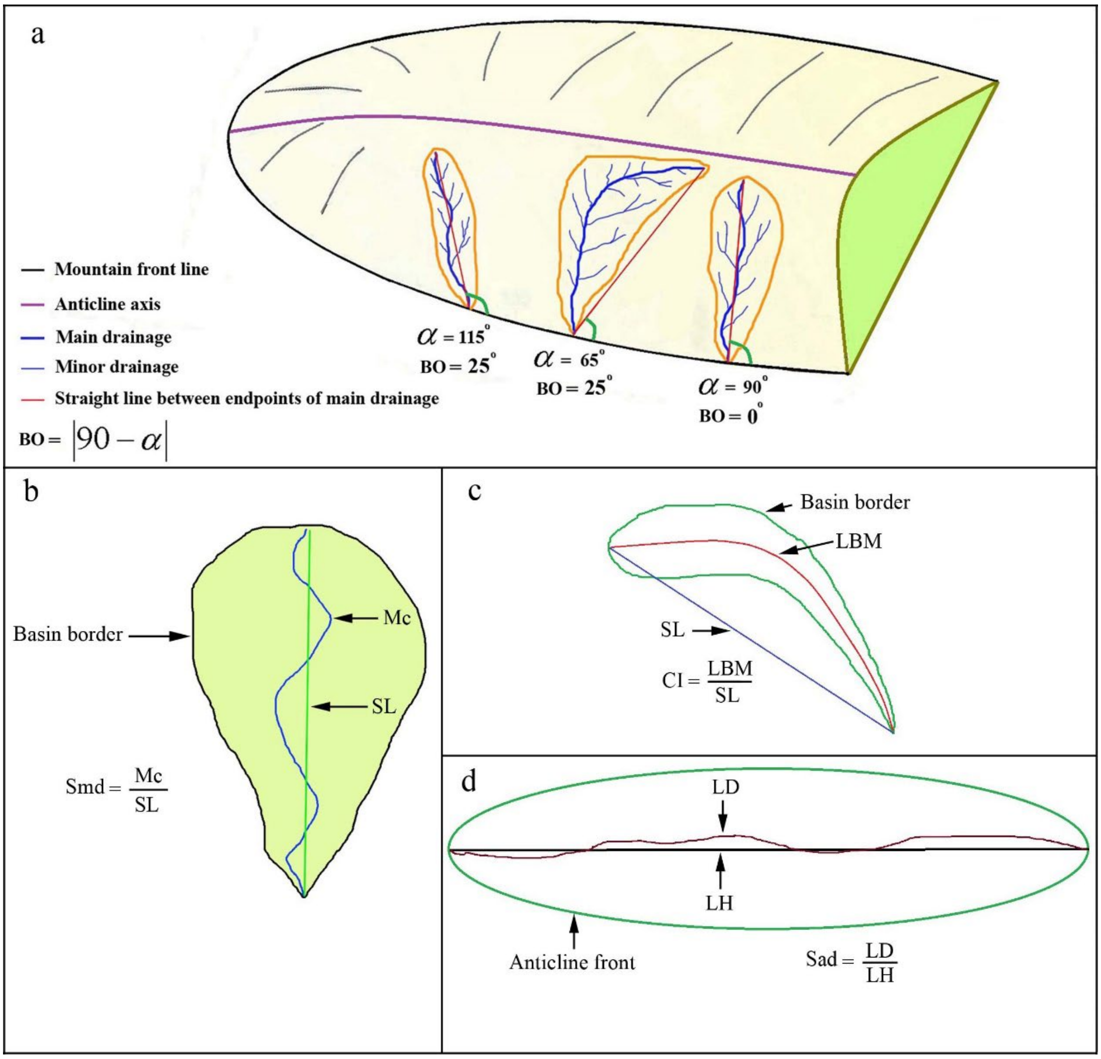
a
Mountain front line
Anticline axis
Main drainage
Minor drainage
Straight line between endpoints of main drainage
$\alpha = 115^\circ$
BO = 25°
$\alpha = 65^\circ$
BO = 25°
$\alpha = 90^\circ$
BO = 0°
$BO = |90 - \alpha|$
b
Basin border
Mc
SL
$Smd = \frac{Mc}{SL}$
c
Basin border
LBM
SL
$CI = \frac{LBM}{SL}$
d
LD
LH
Anticline front
$Sad = \frac{LD}{LH}$

Fig. 7

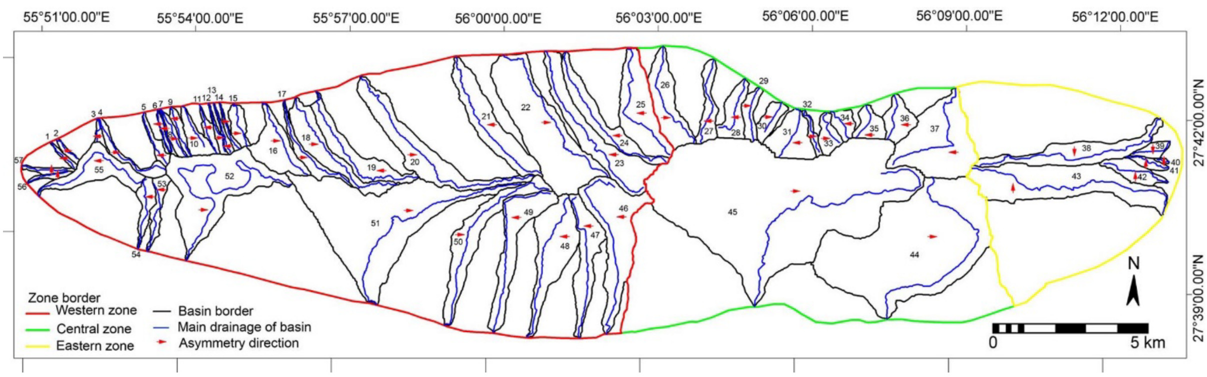
55°51'00.00"E
55°54'00.00"E
55°57'00.00"E
56°00'00.00"E
56°03'00.00"E
56°06'00.00"E
56°09'00.00"E
56°12'00.00"E
27°42'00.00"N
27°39'00.00"N
Zone border
Western zone
Central zone
Eastern zone
Basin border
Main drainage of basin
Asymmetry direction
N
0
5 km

Fig. 8

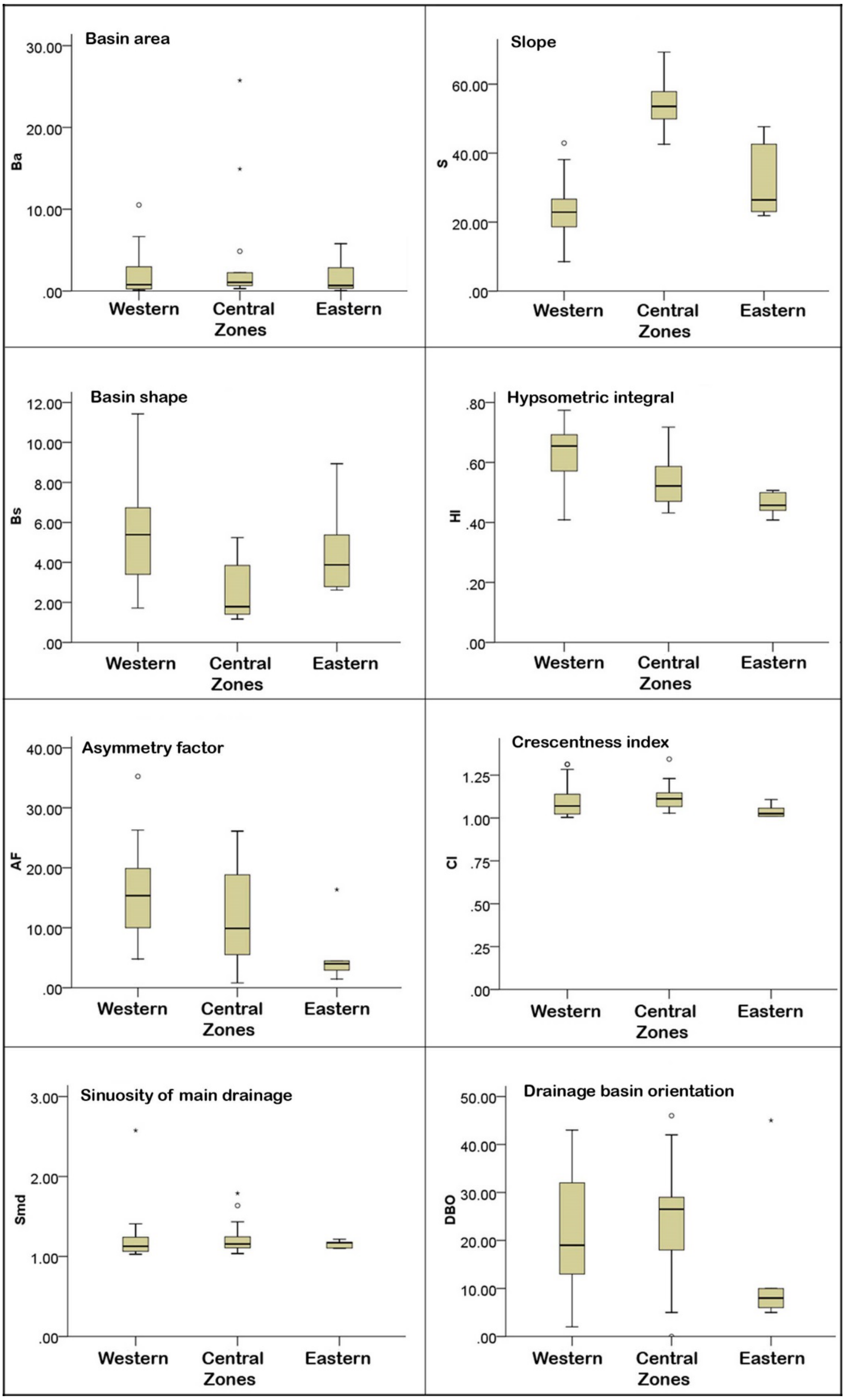
Basin area
Ba
30.00
20.00
10.00
.00
Western
Central
Zones
Eastern
Slope
S
60.00
40.00
20.00
.00
Western
Central
Zones
Eastern
Basin shape
Bs
12.00
10.00
8.00
6.00
4.00
2.00
.00
Western
Central
Zones
Eastern
Hypsometric integral
HI
.80
.60
.40
.20
.00
Western
Central
Zones
Eastern
Asymmetry factor
AF
40.00
30.00
20.00
10.00
.00
Western
Central
Zones
Eastern
Crescentness index
CI
1.25
1.00
.75
.50
.25
.00
Western
Central
Zones
Eastern
Sinuosity of main drainage
Smd
3.00
2.00
1.00
.00
Western
Central
Zones
Eastern
Drainage basin orientation
DBO
50.00
40.00
30.00
20.00
10.00
.00
Western
Central
Zones
Eastern

Fig. 9

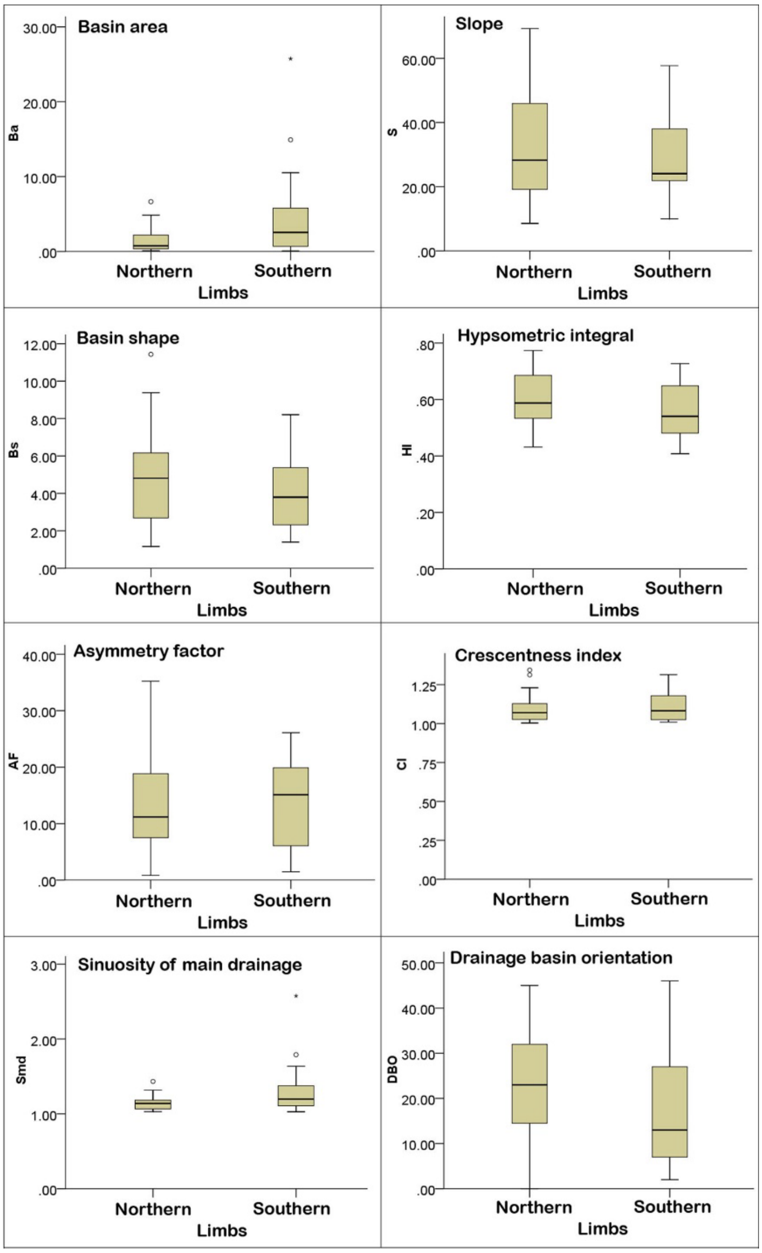
Basin area
Ba
Slope
S
Basin shape
Bs
Hypsometric integral
HI
Asymmetry factor
AF
Crescentness index
CI
Sinuosity of main drainage
Smd
Drainage basin orientation
DBO
Northern
Southern
Limbs

Fig. 10

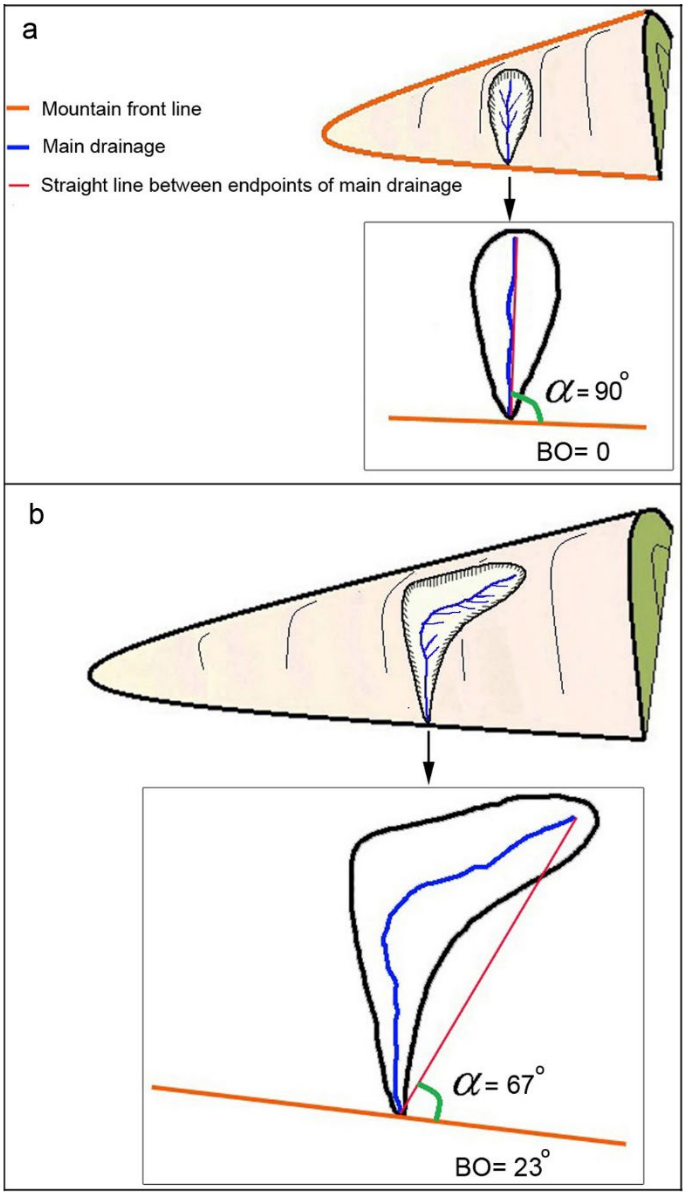
a
Mountain front line
Main drainage
Straight line between endpoints of main drainage
α = 90°
BO= 0
b
α = 67°
BO= 23°

Fig. 11

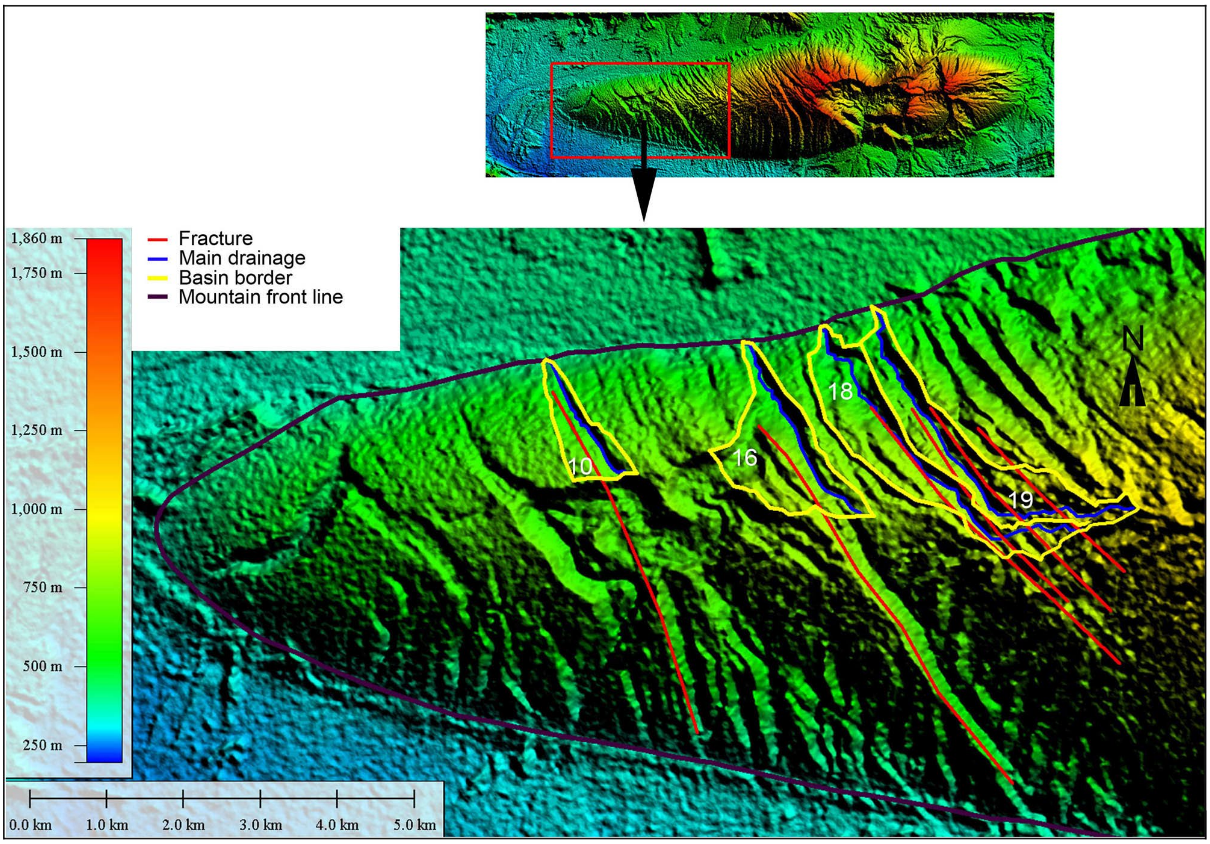
1,860 m
1,750 m
1,500 m
1,250 m
1,000 m
750 m
500 m
250 m
Fracture
Main drainage
Basin border
Mountain front line
10
16
18
19
N
0.0 km
1.0 km
2.0 km
3.0 km
4.0 km
5.0 km

Fig. 12

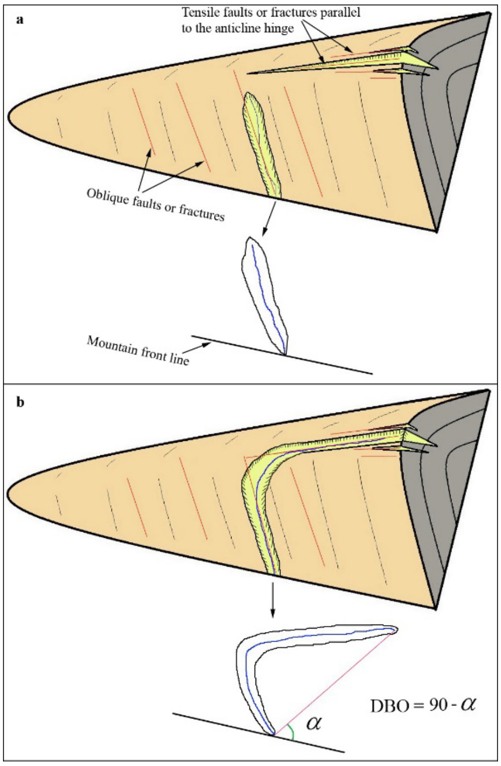
a
Tensile faults or fractures parallel to the anticline hinge
Oblique faults or fractures
Mountain front line
b
α
DBO = 90 - α

Fig. 13

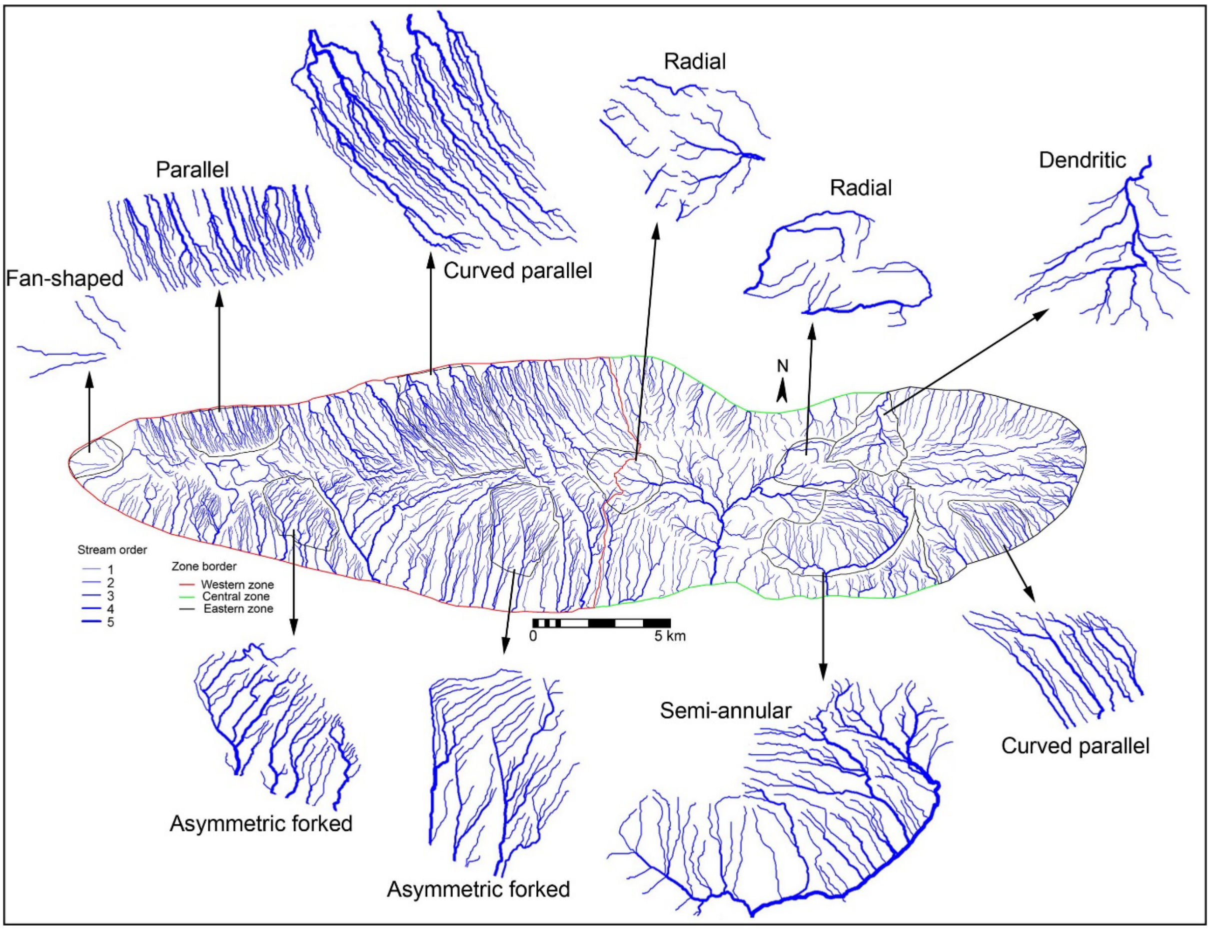

Radial
Parallel
Radial
Dendritic
Fan-shaped
Curved parallel
N
Stream order
1
2
3
4
5
Zone border
Western zone
Central zone
Eastern zone
0
5 km
Semi-annular
Curved parallel
Asymmetric forked
Asymmetric forked

Fig. 14